Title page

Debonding strength evaluation in terms of the intensity of singular stress at the interface corner with and without fictitious crack

Nao-Aki Noda [a,*], Tatsujiro Miyazaki [b], Rong Li [c], Takumi Uchikoba [c], Yoshikazu Sano [a] and Yasushi Takase [a]

[a] Department of Mechanical Engineering, Kyushu Institute of Technology, 1-1 Sensui-cho, Tobata-ku, Kitakyushu-shi, Fukuoka 804-8550, Japan

[b] Department of Mechanical Systems Engineering, University of the Ryukyus, 1 Senbaru, Nishihara-cho, Nakagami-gun, Okinawa 903-0213, Japan

[c] Department of Mechanical Engineering, Graduate School of Engineering, Kyushu Institute of Technology, 1-1 Sensui-cho, Tobata-ku, Kitakyushu-shi, Fukuoka 804-8550, Japan

*Corresponding author: Nao-Aki NODA, Department of Mechanical Engineering, Kyushu Institute of Technology, 1-1 Sensui-cho, Tobata-ku, Kitakyushu-shi, Fukuoka 804-8550, Japan, Tel: +81-080-3886-6069, E-mail: noda@mech.kyutech.ac.jp

Abstract

In this study the debonding strength of adhesively bonded joints is investigated in terms of the intensities of the singular stress fields at the ends of the joints. First, a homogeneous and flawless elastic adhesive layer is assumed to evaluate the butt joint strength for carbon steel/epoxy resin, aluminum/araldite, and brass/solder. It is found that the adhesive strength is always expressed as the critical intensities of singular stress. Next, a small fictitious interface edge crack is assumed at the adhesive layer considering double singular stress fields including and excluding the crack. Then the debonding strength is also found to be controlled by the critical interface stress intensity factor of the fictitious crack. A suitable dimension of the fictitious crack is discussed to predict the strength for adhesive joints accurately and conveniently.

Keywords

Adhesion; Fracture mechanics; Stress intensity factor; Interfaces; Crack

Nomenclature

a　　　　length of the edge interface crack

C_I, C_{II}　　constants for mode I, mode II defined as $C_I = F_I \left(\dfrac{a}{W} \right)^{1-\lambda}, C_{II} = F_{II} \left(\dfrac{a}{W} \right)^{1-\lambda}$

E　　　　Young's modulus

F_σ　　　dimensionless corner stress intensity factor

F_I, F_{II} dimensionless interface stress intensity factors for mode I, mode II

F_{I,λ_1} dimensionless notch stress intensity factor for mode I

G shear modulus

h adhesive thickness

K_σ corner stress intensity factor

$K_{\sigma c}$ critical value of corner stress intensity factor

K_I, K_{II} interface stress intensity factors for mode I, mode II

K_{IC} critical value of interface stress intensity factor for mode I

K_{I,λ_1} notch stress intensity factor for mode I

K_{IC,λ_1} critical value of notch stress intensity factor for mode I

r radial distance away from the singular point/crack tip

W width of the bonded strip

M bending moment applied

t depth of notch

T, S tensile and shear stresses applied to the reference problem

$f_{ij}(\theta)$ angle functions expressing singular stress field

α, β Dundurs' material composite parameters

γ notch opening angle (degrees)

ε bi-elastic constant

θ angle from the interface corner

λ singular index

σ_c adhesive strength

σ_y, τ_{xy} tension and shear stress component near the crack tip

$\sigma_y^\infty, \tau_{xy}^\infty$ tension and shear stress at infinity

$\sigma_{yo}^{FEM*}, \tau_{xyo}^{FEM*}$ finite element stresses at the crack tip of the reference problem

$\sigma_{yo}^{FEM}, \tau_{xyo}^{FEM}$ finite element stresses at the crack tip of the given unknown problem

v Poisson's ratio

1. Introduction

Adhesively bonded joints are economical, practical and easy to make; thus they have been widely used in a variety of industries [1-9], such as integrated circuit (IC) technology. With the development of IC technology, the size of IC chip has been enlarged, and the package has been made thinner and smaller. It has been reported that when a plastic IC package is in the thermal environment or subjected to mechanical loading, the interfacial debonding often occurs [10-13]. So the debonding evaluation has become more and more an important issue in the design of IC packages. However, due to the mathematical difficulties, few analytical methods are available for interfacial debonding, and a more practical and rational method is required.

A number of studies on debonding strength have been made so far [14-16]. Naito investigated the geometrical effect of adhesive thickness on the tensile and shear strength for butt and single lap joints [5]. It is known that the adhesive strength σ_c

increases with decreasing the adhesive thickness [2-5]. The previous studies suggested this is because more defects and cavities are included in the thick adhesive layer [17]. The experimental studies also suggested that the residual strain of adhesive layer may affect the results [18-21]. Suzuki discussed the experimental adhesive strength in Fig.1 (a) when S35C JIS medium carbon steel plates are bonded by epoxy resin [22]. In this study, the specimens are very carefully prepared to exclude the defect and residual strain. Therefore in this paper, first, we consider Suzuki's results because the defect and residual strain may be excluded in the experiment.

Recently the authors have found that the intensity of the singular stress in Fig.1 (b) decreases with decreasing the adhesive thickness [23]. The authors have also shown the solution for small edge interface crack [24-26] and clarified material combinations effects [26-30]. In this study, therefore, debonding criterion will be considered in terms of the intensities of the singular stress based on the solutions. Therefore two models are considered: one is the perfectly-bonded model as shown in Fig.1 (b), and the other is fictitious crack model as shown in Fig.1(c). Then the critical debonding conditions will be discussed.

Generally speaking, there are two types of approaches to explain the adhesive strength:

(1) Effect of dimension of adhesive layer is mainly considered assuming homogeneous adhesive layer without focusing on defects and residual strain.

(2) Effect of non-homogeneity such as defect and residual strain in the adhesive layer is mainly considered without focusing on the geometrical effects.

One may think the most useful approach would certainly account for both geometry and defects. However, for example, in standard fracture mechanics approach, a cracked homogeneous elastic body is usually considered without considering any other defects. In this sense, in this study, to evaluate the adhesive strength simply and conveniently, we will focus on the intensity of singular stress based on the approach (1) without considering other defects and residual strain. Then, if something cannot be explained, approach (2) should be considered in the future, the authors think.

2. Convenient analysis method for the corner stress intensity factor

Here, we consider Fig.2 to explain the outline of the method of analysis for the corner stress intensity factor. The details are indicated in [23, 28, 29]. For the adhesive joint as shown in Fig.2, it is known that the interface stress σ_y has singularity in the form $\sigma_y \propto 1/r^{1-\lambda}$ when $\alpha(\alpha - 2\beta) > 0$. Here, α, β denote the Dundurs' material composite parameters defined in Eq. (1).

$$\alpha = \frac{G_1(\kappa_2 + 1) - G_2(\kappa_1 + 1)}{G_1(\kappa_2 + 1) + G_2(\kappa_1 + 1)}, \beta = \frac{G_1(\kappa_2 - 1) - G_2(\kappa_1 - 1)}{G_1(\kappa_2 + 1) + G_2(\kappa_1 + 1)}, \kappa_j = \begin{cases} \dfrac{3 - \nu_j}{1 + \nu_j} & (\text{plane stress}) \\ 3 - 4\nu_j & (\text{plane strain}) \end{cases} \quad (j = 1,2) \quad (1)$$

The notation λ in Table 1 denotes the singular index, and the values of λ can be determined from Eq. (2) [31, 32].

$$\left[\sin^2\left(\frac{\pi}{2}\lambda\right)-\lambda^2\right]^2\beta^2+2\lambda^2\left[\sin^2\left(\frac{\pi}{2}\lambda\right)-\lambda^2\right]\alpha\beta+\lambda^2\left(\lambda^2-1\right)\alpha^2+\frac{\sin^2(\pi\lambda)}{4}=0 \qquad (2)$$

When the singularity exists near the interface corner, the minimum root λ in Eq. (2) should be in the range $0\le\mathrm{Re}(\lambda)\le1$. The corner stress intensity factor K_σ at the adhesive dissimilar joint is defined as

$$K_\sigma=\lim_{r\to0}\left[r^{1-\lambda}\times\sigma_y^{real}(r)\right]. \qquad (3)$$

The dimensionless of dimensionless corner stress intensity factor F_σ is defined by the following equation [23].

$$F_\sigma=\frac{K_\sigma}{\sigma_y^\infty(W)^{1-\lambda}}=\frac{\lim_{r\to0}\left[r^{1-\lambda}\times\sigma_y^{real}(r)\right]}{\sigma_y^\infty(W)^{1-\lambda}} \qquad (4)$$

Table 2 shows the stress σ_y^{FEM} obtained by applying the finite element method (FEM) when $h/W=0.001$ and $h/W\ge1$ since the reference problem for $h/W\ge1$ has the exact solution [33]. It is seen that σ_y^{FEM} varies depending on the finite element mesh size due to the singularity of the real stress σ_y^{real}.

$$K_\sigma\ne\lim_{r\to0}\left[r^{1-\lambda}\times\sigma_y^{FEM}(r)\right] \qquad (5)$$

Therefore, we consider the ratio $\sigma_y^{FEM}/\sigma_{y*}^{FEM}$ since the error is controlled by the mesh size. It should be noted that the ratio of the stress is independent of the mesh size.

As shown in Eq. (6), the ratio of corner stress intensity factor K_σ^*/K_σ is controlled by the ratio of stress $\lim_{r\to0}[\sigma_y^*(r)/\sigma_y(r)]$. Here, an asterisk (*) means the values of the reference problem.

$$\frac{K_\sigma^*}{K_\sigma} = \frac{\sigma_y^{\infty*}(W)^{1-\lambda}F_\sigma^*}{\sigma_y^\infty(W)^{1-\lambda}F_\sigma} = \frac{F_\sigma^*}{F_\sigma} = \lim_{r \to 0}\frac{\left[r^{1-\lambda} \times \sigma_y^{FEM\,*}(r)\right]}{\left[r^{1-\lambda} \times \sigma_y^{FEM}(r)\right]} \qquad (6)$$

To obtain the corner stress intensity factor from the ratio, a reference problem as shown in Fig.2 will be used because the exact corner stress intensity factor has been investigated. The authors think this method shown above is convenient to analyze the corner stress intensity factors.

3. Adhesive strength expressed as a constant corner stress intensity factor $K_{\sigma c}$

In this study, the adhesively bonded specimens used by Suzuki [22] in Fig.1 are analyzed where the adherents S35C are bonded with adhesive epoxy resin. In this experiment, the authors prepared for the specimen very carefully to exclude the defect and residual strain. The adhesive was treated with vacuum degassing, and then kept at room temperature for 50-60 days. The Young's modulus of the epoxy adhesive may depend on the constituents of the particle size, material, grain form, dispersant and hardening condition. The difference between epoxy adhesive A, B may be depending on these factors but they are not described in detail. Here, in order to evaluate the adhesive strength conveniently, we consider the average elastic properties of epoxy including fillers. The elastic parameters of the adherent and adhesives are tabulated in Table 1. In this study, the experimental strength value σ_c is the maximum value of average axial stress obtained by dividing the tensile load by the area of the specimen cross section

normal to the load. The load-strain relations are all linear up to the breaking point, which shows that brittle fracture occurred [22]. The fracture was initiated in the vicinity of the adherent surface of either one of the corners of the adhesion plane [22].

The experimental tensile adhesive strength shown in Fig.1 (a) are tabulated in Table 3 with different thicknesses of adhesive layer (h = 0.05, 0.1, 0.3, 0.6, 1.0, 2.0, 5.0 [mm]). As shown in Table 3, with decreasing adhesive thickness, the bond strength increases gradually. The previous studies suggested that since the residual strain and defect are included in adhesive layer, the strength may decrease when adhesive thickness is thin enough [18, 34]. In this research, in order to explain the results of Table 3 conveniently, we assume the adhesive layer as a homogeneous material assuming no defect and residual strain.

The analytical values of F_σ are listed in Table 4, which are dimensionless corner stress intensity factor obtained by using the calculation method in Section 2 with varying the adhesive thickness h in Fig.1 (b). Then the critical values of the corner stress intensity factor $K_{\sigma c}$ are tabulated in Table 4 [see Eq. (7)].

$$K_{\sigma c} = F_\sigma \sigma_c W^{1-\lambda} \tag{7}$$

Furthermore, the relationship between $K_{\sigma c}$ and the thickness of adhesive layer h is plotted in Fig.3 [23]. Here, the open circles denote $K_{\sigma c}$ values obtained from experiment, the solid circles denote the average value of $K_{\sigma c}$ for each h/W, and the solid line shows the average value of the solid circles. Fig. 3 shows that the solid circles

are distributed around the solid line with slight variations. Table 4 indicates the average and standard deviation of the critical intensity as $K_{\sigma c} = 1.04 \pm 0.0643 \, [\text{MPa} \cdot \text{m}^{0.315}]$ for S35C steel/Epoxy A (Combination A, see Table 1) and $K_{\sigma c} = 1.20 \pm 0.144 \, [\text{MPa} \cdot \text{m}^{0.326}]$ for S35C steel/Epoxy B (Combination B, see Table 1). The coefficients of variations are 0.0618 for Combination A, and 0.120 for Combination B, which are defined as the standard deviation/ average.

Fig. 4 shows the results obtained for Aluminum/Araldite and Brass/Solder as indicated in Table 5 as Combinations C and D. The adhesive strengths σ_c were obtained from Akisanya and Meng [35]. Microscopic examination of the fracture surface revealed that failure occurred at the interface corner and the initiated crack grew along the interface in both Combinations C and D. Table 6 shows the average and standard deviation as $K_{\sigma c} = 0.609 \pm 0.0475 \, [\text{MPa} \cdot \text{m}^{0.286}]$ for Combination C and $K_{\sigma c} = 4.80 \pm 0.780 \, [\text{MPa} \cdot \text{m}^{0.255}]$ for Combination D. The coefficients of variations are 0.0780, 0.163.

From Fig.3 and Fig.4, it is seen that the adhesive strength can be evaluated by the constant corner stress intensity factor as $K_{\sigma c}$ =const. Meanwhile, Suzuki's results were evaluated in terms of H singular stress and expressed as H_{cr} =const [36, 37]. Furthermore, H_{cr} criterion is also applied to evaluate scarf joint. However, local geometrical difference disables us for comparing those results because of different singular index singular fields [38-41]. On the other hand, the fictitious crack model

enables us to compare the results independent of the local geometrical difference. In the following, we will focus on the application of the fictitious crack model.

Akisanya and Meng [35] state that in the case of Brass/Solder joint, the stress intensity factor is not suitable to characterize the initiation of fracture because of the large plastic zone size. However, Fig.4 (b) shows the adhesive strength can be expressed almost as a constant critical value of corner stress intensity factor $K_{\sigma c}$. Usually, in the fracture mechanics approach, the small size of plastic zone is necessary and known as small scale yielding condition. However, in the present approach, we considered the singular stress at the interface. In this case, the yielding condition is not clear because two different material characters should be considered and the real interface and the model's interface may be different. Therefore, in this study, the elastic singular stress is discussed. Then, if something cannot be explained in the future by this approach, plasticity should be considered, the authors think.

4. Convenient analysis method for interface crack

Here, we consider Fig.5 to explain the outline of the method of analysis for interface crack. The details are indicated in [24, 25, 42, 43]. The two different interface crack problems A and B in Fig. 5 have the same crack length a and the same combination of material ε, assuming the interface stress intensity factor of problem A is available and those for problem B are yet to be solved. Problem A is the reference problem whose

values are marked with *, and problem B is the given unknown problem. Then, the problems A and B are solved by applying the same FEM mesh pattern around the interface crack tip.

The analytical solution of the singular stress factors at the crack tip for the reference problem takes the form

$$K_I^* + iK_{II}^* = (T + iS)\sqrt{\pi a}(1 + 2i\varepsilon) , \tag{8}$$

where T, S are the remote uniform tension and shear applied to the bonded dissimilar half-planes.

The stresses at the crack tip of the reference problem are expressed as

$$\sigma_{y0}^{FEM} * = \sigma_{y0}^{FEM} *|_{T=1,S=0} \times T + \sigma_{y0}^{FEM} *|_{T=0,S=1} \times S ,$$

$$\tau_{xy0}^{FEM} * = \tau_{xy0}^{FEM} *|_{T=1,S=0} \times T + \tau_{xy0}^{FEM} *|_{T=0,S=1} \times S . \tag{9}$$

Then, the finite element stress components at the crack tip for the problems A and B have relation

$$\begin{bmatrix} \tau_{xy0}^{FEM} * \\ \sigma_{y0}^{FEM} * \end{bmatrix}_A = \begin{bmatrix} \tau_{xy0}^{FEM} \\ \sigma_{y0}^{FEM} \end{bmatrix}_B \tag{10}$$

Let $T=1$, the value of S can be determined as

$$S = \frac{\sigma_{y0}^{FEM} \times \tau_{xy0}^{FEM} *|_{T=1,S=0} - \tau_{xy0}^{FEM} \times \sigma_{y0}^{FEM} *|_{T=1,S=0}}{\tau_{xy0}^{FEM} \times \sigma_{y0}^{FEM} *|_{T=0,S=1} - \sigma_{y0}^{FEM} \times \tau_{xy0}^{FEM} *|_{T=0,S=1}} . \tag{11}$$

Finally, the singular intensity factors for the given unknown problem B can be yielded using the proportional relationship as given in Eq. (12).

$$[K_I]_B = \frac{[\sigma_{y0}^{FEM}]_B}{[\sigma_{y0}^{FEM} *]_A}[K_I^*]_A, \quad [K_{II}]_B = \frac{[\tau_{xy0}^{FEM}]_B}{[\tau_{xy0}^{FEM} *]_A}[K_{II}^*]_A \tag{12}$$

Fig.6 shows the stress distributions near the interface crack tip for problems A and B if Eq. (9) and Eq. (10) are satisfied. It is seen that the singular stress field of the interface crack is controlled by $\tau_{xyo}^{FEM} / \sigma_{yo}^{FEM}$ at the crack tip. The authors think this method is convenient to analyze the interface stress intensity factors.

5. Usefulness of fictitious crack model

In general, singular stress field near edge interface can be expressed as shown in the following equation by using three terms, that is, (A) singular index λ_m, (B) angle function with vertices singularity $f_{ij}(\theta)$, (C) stress intensity factor K_m .

$$\sigma_{ij}(r,\theta) = \sum_{m=1} \frac{K_m}{r^{1-\lambda_m}} f_{ij}(\theta), \ (ij = r,\theta,r\theta) \tag{13}$$

Singular indexes λ_m may be obtained from solving the characteristic equation, which expresses geometrical boundary conditions around the singular point. The roots λ_m can be single or multiple real roots as expressed in equation (2); and the roots can be complex roots expressed by different types of equations.

Consider an IC package as shown in Fig. 7. To evaluate the interface strength, we have to calculate K_m considering distinct singular index λ_m and angle function $f_{ij}(\theta)$ at five points A to E. Although the material combinations are the same at points A, B, C, the singular indexes λ_m at points A, B, C are different as well as the angle functions $f_{ij}(\theta)$ and intensities K_m .

In this way, the singular stress field for dissimilar materials bonded interface varies

depending on the geometry and material combination, and therefore it is difficult to compare the intensities.

The fictitious crack model as shown in Fig.1(c) has some advantages when we have to compare the interface strength at points A, B, and C. A fictitious crack is not a real debonding. A fictitious crack is just used to evaluate the severity at the end of the interface. This is because the interface crack always has the distinct singular stress field, whose singular index is $\lambda = 1/2 + i\varepsilon$ and expressed in Eq. (14) [24-28, 30, 42, 43].

$$\left[\sigma_y + i\tau_{xy}\right]_{\theta=0} = \frac{K_I + iK_{II}}{\sqrt{2\pi r}} \left(\frac{r}{a}\right)^{i\varepsilon}, \ \varepsilon = \frac{1}{2\pi} \ln\left(\frac{1-\beta}{1+\beta}\right) \tag{14}$$

$$K_I + iK_{II} = \left(F_I + iF_{II}\right) \sigma_y^\infty \sqrt{\pi a} \tag{15}$$

Here, K_I and K_{II} are the interface stress intensity factors. The real part of the singular index $\lambda = 1/2$ is independent of the shape of the edge interface and also independent of the material combination. Since the singular stress of edge interface is expressed by the unified singular stress field, the advantage of assuming fictitious crack model can be summarized as follows [44, 45].

(1) The distinct singular stress field as Eq. (13) is not necessarily to be obtained. Although the points A, B, C have distinct singular fields, assumed fictitious cracks always provide the same singular fields in Eq. (14) [26,42,43] (see Fig.7(b)).

(2) If the critical value of the interface stress intensity factor is available at A, for example, the results can be applied to other points B and C since they have the same singular fields.

6. An example of fictitious crack model application

By taking an example of V-shaped notch problem in Fig.8, the usefulness of the fictitious crack will be explained. The details are indicated in [39-41]. First, the static tensile strength of notched acrylic resin plate will be discussed by applying the notch stress intensity factors K_{I,λ_1} without using fictitious crack.

The singular stress at the sharp V-notch can be expressed in Eq. (16) [46].

$$\sigma_{ij} = f_{ij}^I (\theta) \frac{K_{I,\lambda_1}}{r^{1-\lambda_1}}$$
$$= \frac{\lambda_1}{\sqrt{2\pi}} \{(\lambda_1 +1)\sin[\lambda_1(\pi - \gamma)] - \lambda_1 \sin[\lambda_1(\pi - \gamma) + \gamma] + \sin(\lambda_1 \pi)\} \frac{K_{I,\lambda_1}}{r^{1-\lambda_1}} \tag{16}$$

In Eq. (16), the singular stress field around the notch tip is defined in terms of notch stress intensity factor K_{I,λ_1}, which is defined in Eq. (17).

$$K_{I,\lambda_1} = \lim_{r \to 0} [\sqrt{2\pi} r^{1-\lambda_1} \sigma_\theta(r,\theta)|_{\theta=0}] \tag{17}$$

Here, $\sigma_\theta(r,\theta)|_{\theta=0}$ is the stress along the bisector of the notch, and λ_1 is the singularity index, in the range of $0 < \lambda < 1$, obtained from the following eigenequation:

$$\sin\left[\lambda_1 (2\pi - \gamma)\right] = \lambda_1 \sin\gamma . \tag{18}$$

The notch stress intensity factor K_{I,λ_1} can be expressed in Eq. (19) [46]. Several dimensionless notch stress intensity factors F_{I,λ_1} are indicated in [39-41, 46-50].

$$K_{I,\lambda_1} = F_{I,\lambda_1} \sigma^\infty \sqrt{\pi} t^{1-\lambda_1}, \ \sigma^\infty = \begin{cases} \sigma_y^\infty & : \text{Tension} \\ 6M / W^2 & : \text{Bending} \end{cases} \tag{19}$$

Fig.9 shows the critical value K_{IC,λ_1} experimentally obtained, which is necessary to

fracture the specimens with the same notch opening angle $\gamma = 60^o$. As shown in Fig.9, it is found that K_{IC,λ_1} is almost constant independent of the notch depth t/W and whether the notch is single or double.

Fig.10 shows the experimental results of K_{IC,λ_1} with various notch opening angles γ. The value is depending on the notch opening angle γ which has distinct singular stress index λ_1. As shown in Table 7, the value of λ_1 increases with increasing the notch opening angle γ. On this sense, the sharp V-notch fracture problem is different from the crack fracture problem because the critical value of notch stress intensity factors necessary to notch fracture is a function of the notch opening angle γ. Thus, even for mode I fracture problem, many data of K_{I,λ_1} are necessary under different notch opening angle although only K_{IC} can be applied to all the crack problems.

Therefore, another fracture criterion using fictitious crack is useful in application [39-41]. Here, the critical values of stress intensity factors can be estimated from the mechanical properties of the considered material such as the tensile strength σ_B or the critical value of stress intensity factor K_{IC}.

In Fig.11, a fictitious crack is considered at the notch tip. Here, the fracture at the notch tip is simulated by propagation of this small fictitious crack, with a length of "a", imagined at the notch tip. Fracture occurs when the stress intensity factor at the crack tip K_I is larger than the critical value K_{IC} [see Eq. (20)].

$$K_I\big|_{r=a} \geq K_{IC} \tag{20}$$

The crack length "a" obtained by Eq.(20) is related to the fracture process zone size.

The fracture strength for the sharp notch specimen is discussed by using the stress intensity factor of small fictitious crack. The dimensionless stress intensity factor F_I at the crack tip is expressed as shown in Eq.(21) by using the stress $\sigma_y(a)$ ahead of the notch without crack as shown in Fig.11 [41].

$$F_I = \frac{K_I}{\sigma_y(a)\sqrt{\pi a}} = \frac{K_I}{K_{I,\lambda_1}}a^{0.5-\lambda_1} \tag{21}$$

Therefore the fracture criterion Eq.(20) can be expressed as

$$K_I\big|_{r=a} = F_I a^{\lambda_1-0.5}K_{I,\lambda_1} \geq K_{IC}. \tag{22}$$

The dimensionless stress intensity factor and singularity index are tabulated in Table.8. Here, the F_I decreases with increasing the notch opening angle γ. Fig.12 indicates that F_I for $\gamma = 90^{\circ}$ has the same value when $a/t \leq 0.005$ independent of t/W.

The relationships between the critical value of stress intensity factor K_{IC} and t/W are plotted in Fig.13 for $a/t = 0.005$. It is found that the K_{IC} is almost constant independent of a/t and opening angle γ. In this case, all sharp V-notch fractures can be expressed as $K_{IC} = 37.1\text{N/mm}^{1.5}$ independent of notch opening angle γ and notch depth t assuming the fictitious crack length $a/t = 0.005$. In Fig.14 a suitable fictitious crack length is discussed by comparing the predicted K_{I,λ_1} obtained from Eq.(22) $K_I\big|_{r=a} \geq K_{IC}$ with the experimental value [40]. It is seen that the predicted K_{I,λ_1} is insensitive to the crack length "a" since the value is almost constant except for very

small value of "a". In [40] a fictitious crack whose length $a = 0.042 - 0.166$mm is found to be suitable, but Fig.13 shows smaller values of $a = 0.02$mm~ also can be used with $K_{IC} = 37.1$N/mm$^{1.5}$.

7. Adhesive strength expressed as a constant interface stress intensity factor K_{IC} by assuming fictitious crack

The calculation method described in Section 5 and [24, 25] is applied and the dimensionless interface stress intensity factors F_I are listed with the ratio F_{II}/F_I in Table 9 under $a/W = 0.01$, 0.1. Except for the extremely thin adhesive layer, it is seen that the debonding strength can be expressed as a constant value of K_{IC}. Since the value of F_{II}/F_I is also almost constant regardless of a/W, the critical values of the mode I interface stress intensity factors K_{IC} are tabulated in Table 9 [see Eq. (23)].

$$K_{IC} = F_I \sigma_c \sqrt{\pi a} \tag{23}$$

The relationships between the critical interface stress intensity factors K_{IC} and the adhesive thickness h are plotted in Fig.15 for $a/W = 0.01$ and in Fig.16 for $a/W = 0.1$.

As shown in Table 9, when $a/W = 0.01$, the average value and standard deviations $K_{IC} = 0.446 \pm 0.0356$ [MPa$\sqrt{m}$] for Combination A, and $K_{IC} = 0.551 \pm 0.0576$ [MPa$\sqrt{m}$] for Combination B. The coefficients of variation are 0.0789 and 0.105, respectively. When $a/W = 0.1$, the average value and standard deviations $K_{IC} = 0.844 \pm 0.0517$ [MPa$\sqrt{m}$] for Combination A, and $K_{IC} = 1.01 \pm 0.107$ [MPa$\sqrt{m}$] for Combination B. The coefficients

of variation are 0.0603 and 0.106, respectively. It is seen that the adhesive strength can

be evaluated from the critical value of interface stress intensity factor K_{IC}=const.

In a similar way, Akisanya's results are indicated in Table 10, Fig.17 and Fig.18.

From the comparison between Tables 4, 6, 9, 10 and Figs. 3, 4, 15-18, no significant

difference can be seen for the variation between the $K_{\sigma c}$ and the K_{IC}. In other words,

there is no large difference between the results from the perfectly bonded model and the

fictitious crack model.

8. Adhesive strength predicted by assuming different fictitious crack lengths

The previous section shows that the adhesive strength can be evaluated accurately,

even though $a/W = 0.1$ is not very small as the fictitious crack length. In this section, we

discuss the suitable length of the fictitious crack based on the interface stress intensity

factor [26]. Fig. 19 shows F_I vs. a/W for the geometry of Fig.1 (c). The F_I value

goes to infinity as $a/W \to 0$. This is due to the singular stress appearing at the end of

interface when there is no crack. Therefore the following constant C_I should be

introduced because C_I takes a constant value as $a/W \to 0$ [26]. The detail explanation

of the constant C_I is shown in the Appendix B [26].

$$C_I = F_I \left(\frac{a}{W} \right)^{1-\lambda}$$

(24)

Fig. 20 shows C_I vs. a/W for Fig.1 (c) based on the results in Table 11. When the

crack length is sufficiently small compared to the thickness of the adhesive layer, the C_I value is almost constant. The interface stress intensity factor can be expressed as shown in Eq. (25).

$$K_I = F_I \sigma \sqrt{\pi a} = C_I \left(\frac{W}{a}\right)^{1-\lambda} \sigma \sqrt{\pi a}$$
$$= \frac{C_I}{F_\sigma} \frac{F_\sigma W^{1-\lambda} \sigma}{a^{1-\lambda}} \sqrt{\pi a} = \frac{C_I}{F_\sigma} \frac{K_\sigma}{a^{1-\lambda}} \sqrt{\pi a} \qquad (25)$$

As shown in Eq. (25), if the ratio C_I/F_σ is independent of the crack length, K_I is controlled by the stress field without crack K_σ. This means that the short crack is placed at the singular stress field at the interface end. When the adhesive layer is thin, and h/W is small, K_I can be controlled by the singular stress field without crack if we take small a/W. Adhesive strength can be expressed from K_{IC} as shown in Eq. (26).

$$\sigma_c = \frac{K_{\sigma c}}{F_\sigma W^{1-\lambda}} = \frac{K_{IC}}{F_I \sqrt{\pi a}} = \left(\frac{a}{W}\right)^{1-\lambda} \frac{K_{IC}}{C_I \sqrt{\pi a}} \qquad (26)$$

And therefore,

$$K_{IC} = \frac{C_I \sqrt{\pi a}}{F_\sigma a^{1-\lambda}} K_{\sigma c} = \frac{C_I^*}{a^{0.5-\lambda}} K_{\sigma c} = C_I^* K_{\sigma c} a^{\lambda-0.5}, \ C_I^* = \sqrt{\pi} \frac{C_I}{F_\sigma}. \qquad (27)$$

Fig. 21 shows the relation between K_{IC} and "a". Here, it should be noted that this K_{IC} is a fictitious critical intensity factor when a fictitious crack is assumed. To express the same adhesive strength σ_c, the fictitious K_{IC} value increases with increasing the fictitious crack length "a". When $a/W \leq 0.01$ with $W = 12.7\,\text{mm}$, for example, since $\lambda - 0.5 = 0.685 - 0.5 = 0.185$ for Combination A, we have $K_{IC} = C_I^* K_{\sigma c} a^{0.185}$. Since

$C_I^* = \sqrt{\pi}\, C_I / F_\sigma$, if C_I / F_σ is independent of the crack length " a ", we have $K_{IC} \propto a^{\lambda - 0.5} K_{\sigma c}$.

Fig. 22 shows the relationship between C_I / F_σ and a/W . It is found that the adhesive strength can be evaluated conveniently and accurately independent of the fictitious crack length. Furthermore, except for thin adhesive layer, the adhesive strength can be estimated for a wide range of adhesive layer thickness almost independent of fictitious crack length.

Assume debonding happens at the average value of $K_{\sigma c\,(average)}$ obtained in Section 3. Then, Table 12 and Fig. 23 indicate the adhesive strength σ_c , which are calculated from the Eq. (28). The error is also indicated from the comparison of the experimental results σ_c in Table 3.

$$\sigma_c = \frac{K_{\sigma c\,(average)}}{F_\sigma\, W^{1-\lambda}} \tag{28}$$

Assume debonding happens at the fictitious fracture toughness for a/W =0.01, 0.1 obtained in Section 7, Then, Table 12 and Fig. 23 indicate the adhesive strength calculated from Eq. (29). The error is also indicated from the comparison of the experimental results σ_c in Table 3.

$$\sigma_c = \frac{K_{IC(average)}}{F_I\, \sqrt{\pi a}} \tag{29}$$

As shown in Table 12 the error is 11.4% under a/W =0.01 and 10.3% under a/W =0.1 for Combination A, and 16.4% under a/W =0.01 and 14.4% under

$a/W = 0.1$ for Combination B. It is found that the adhesive strength can be predicted with nearly the same accuracy of the perfectly bonded models. The error for Combination B is rather larger compared to the error for Combination A. This is probably because the number of test specimens for Combination B is only three affecting the error. With increasing the number the error may decrease. It may be also concluded that small fictitious crack length provides the same accuracy for the perfectly bonded model.

In this section, the fictitious critical interface stress intensity factor K_{IC} is used to evaluate the adhesive butt joint strength. The fictitious crack length in the range $a/W \leq 0.1$ can be used since the fictitious K_{IC} varies depending on the a/W. If K_{IC} is measured experimentally and used in this evaluation, the crack length a/W should be determined by considering the fracture process zone mentioned in Section 6 without using too small value of a/W. In other words, if real K_{IC} is used, the crack length "a" should be determined from $K_I\big|_{r=a} \geq K_{IC}$. Real K_{IC} may be necessary for evaluating different singular index problems in Fig.7.

9. Conclusion

In this study, several types of adhesive joints are considered in terms of the intensity of singular stress at the interface corner with and without fictitious crack. To evaluate the debonding strength conveniently and efficiently, the elastic and homogeneous

adhesive layer is simply assumed without considering other defects and residual strain. The conclusions can be summarized in the following way.

(1) The corner stress intensity factors K_σ can be obtained conveniently by using the analysis method presented. Then the adhesive strength σ_c for various butt joints can be evaluated as $K_{\sigma c}$ =const for carbon steel/epoxy resin, aluminum/araldite, and brass/solder as shown in Figs.3, 4. As well as the results of Suzuki for carbon steel/epoxy resin [22], whose specimens are carefully prepared to exclude the defect and residual strain, other experimental results can be expressed as the critical stress intensity factor $K_{\sigma c}$ =const.

(2) The interface intensity factors K_I and K_{II} can be obtained conveniently by using the analysis method presented. Then the adhesive strength σ_c for various butt joints can be evaluated as K_{IC} =const assuming fictitious crack modeling as shown in Figs.15 - 18.

(3) The usefulness of the fictitious crack modeling was highlighted by taking an example of sharp V-notch problems. Although different notch opening angle has distinct singular index, the static strength of notched acrylic resin can be expressed as K_{IC} =const. The suitable fictitious crack length is found to be $a =$ 0.02-0.16mm on the basis of the criterion when the fracture occurs at the crack tip as $K_I\big|_{r=a} \geq K_{IC}$.

(4) The relationship between the critical value of interface stress intensity factor K_{IC} and critical value of corner stress intensity factor $K_{\sigma c}$ is considered. The relation $K_{IC} \propto a^{\lambda-0.5} K_{\sigma c}$ can be derived for the fictitious crack length $a/W \leq 0.01$ (see Figs.21, 22).

(5) The suitable dimension for fictitious crack was discussed for butt joints. The applicability should be confirmed in the further studies for other types of joint geometries.

Appendix A. Corner stress intensity factor for bonded strip under arbitrary material combinations

In this paper, the dimensionless corner stress intensity factor F_σ for the perfectly-bonded strip (see Fig. 2(c)) was obtained from our previous study [20]. The analytical values of F_σ are listed as follows.

Table A.1 indicate the results for bonded strip in Fig. 2(d), which are equivalent to the case $h/W \geq 1$. Using the results $F_\sigma \big|_{h/W=1}$ in Table A.1 and $F_\sigma / F_\sigma \big|_{h/W=1}$ in Table A.2, F_σ are obtained and shown in Fig. A.1 for $h/W = 0.001$ and $h/W = 0.1$. From those results the critical values of the corner stress intensity factor $K_{\sigma c}$ can be obtained.

Appendix B. Interface stress intensity factors for shallow interface crack under arbitrary material combinations

In this study, the suitable length of the fictitious crack was discussed through interface stress intensity factor based on our previous study [26]. In that paper, the interface stress intensity factors for the shallow edge interface cracks in a bonded strip as shown in Fig.B.1 were investigated.

The dimensionless interface stress intensity factors F_I and F_{II} are often used to express the results of analysis. However, for the bonded semi-infinite plate ($a/W \to 0$), when $\alpha(\alpha-2\beta)>0$, $F_I \to \infty$ and $F_{II} \to \infty$; when $\alpha(\alpha-2\beta)<0$, $F_I \to 0$ and $F_{II} \to 0$. Therefore, F_I and F_{II} are not suitable for edge interface cracks.

However, as indicated in Fig.B.2, $C_I = F_I / (W/a)^{1-\lambda}$ and $C_{II} = F_{II} / (W/a)^{1-\lambda}$ always have finite values when $a/W \to 0$.

Furthermore, the coefficients C_I and C_{II} are constants depending on the material combination. The results for the two coefficients are plotted and listed in Fig. B.3 (a) and Table.B.1 as well as in Fig. B.3(b) and Table.B.2, respectively.

The authors have indicated that the plus and minus of the slope of each value (F_I, F_{II}) is always controlled by the sign of $\alpha(\alpha-\beta)$ [26]. The results of the parameters in the $\alpha-\beta$ space for the various materials combinations shown in [1] are re-plotted in Fig. B.4 [26].

As can be seen from Fig. B.4, most material combinations are located in the "bad pair" region. However, metal/glass, metal/metal, ceramics/ceramics and glass/glass joints can be found in the "good pair" region.

References

[1] Yuuki R. Mechanics of interface. 1st ed. Baifuukann, Tokyo; 1992 [in Japanese].

[2] Hibino Y. Influence of types and surface treatment of dental alloy and film thickness of cements on bond strength of dental luting cements. J Jpn Soc Dent Mater Devices 1990; 9(6):786-805 [in Japanese].

[3] Asada B, Shinya A, Yokozuka S. Effect of dental adhesive film thickness on bond strength. Adhes Dent 1990;8:201–26 [inJapanese].

[4] Kagawa F, Yamada J, Suzuki T, Hisamitsu H, Wakumoto S. The relationship between film thickness of resin luting cements and bond strength, the influence of thermal stress. Jpn J Conserv Dent 1991;34(2):392–8 [inJapanese].

[5] Naito K, Onta M, Kogo Y. The effect of adhesive thickness on tensile and shear strength of polyimide adhesive. Int J Adhes Adhes 2012;36:77–85.

[6] Liu ZX, Huang YA, Yin ZP, Bennati S, Valvo PS. A general solution for the two-dimensional stress analysis of balanced and unbalanced adhesively bonded joints. Int J Adhes Adhes 2014;54:112–23.

[7] Uddin MA, Ali MY, Chan HP. Achieving optimum adhesion of conductive adhesive bonded flip-chip on flex packages. Rev Adv Mater Sci 2009;21 (2):165–72.

[8] Huang Z, Kumar P, Dutta I, Pang JHL, Sidhu R. A general methodology for calculating mixed mode stress intensity factors and fracture toughness of solder joints with interfacial cracks. Eng Fract Mech 2014;131:9–25.

[9] Kitasako Y, Burrow MF, Nikaido T, Harada N, Inokoshi S, Yamada T, Takatsu T. Shear and tensile bond testing for resin cement evaluation. Dent Mater 1995;11(5–6):298–304.

[10]Yasuda M. Hitachi Technical Report 40. 2003. p. 7–12.

[11]Shibutani T. Evaluation of crack initiation at interfacial edge on the basis of fracture mechanics concept and application to electronics devices (Tutorial Series: Foundations for reliability analysis). J Jpn Inst Electron Packag 2004;7 (7):639–44 [inJapanese].

[12]Hattori T, Sakata S, Hatsuda T, Murakami G. A stress singularity parameter approach for evaluating adhesive strength. JSME Int J Ser 1 Solid Mech Strength Mater 1988;31(4):718–23.

[13]Shiratori M. Problems of joints in packaging of electronic devices. Trans Jpn Soc Mech Eng A 1994;60(577):1905–12 [inJapanese].

[14] Di Pisa C, Aliabadi MH. An efficient BEM formulation for analysis of bond-line cracks in thin walled aircraft structures. Int J Fract 2013;179(1-2):129–45.

[15] Hasebe N, Kato S. Solution of problem of two dissimilar materials bonded at one interface subjected to temperature. Arch Appl Mech 2014;84(6):913–31.

[16] Krishnan A, Roy Xu L. An experimental study on the crack initiation from notches connected to interfaces of bonded bi-materials. Eng Fract Mech 2013;111:65–76.

[17] Ikegami K, Kajiyama M, Kamiko S, Shiratori E. Experimental studies of the strength of an adhesive joint in a state of combined stress. J Adhes 1979;10 (1):25–38.

[18] Yamato T, Shirahama M, Hara S. Effect of adhesive thickness on the strength of chlorinated rubber adhesive. J Soc Rubber Sci Technol 1957;30(11):842–7 [in Japanese].

[19] Yokoyama T, Nakai K, Ikeda T. Effect of specimen geometry on tensile properties of structual adhesive butt joints. In: JSME annual meeting; 2006. p. 861–2 [inJapanese].

[20] Akinmade A O, Nicholson J W. Effect of adhesive layer thickness on the bond strength of a zinc polycarboxylate dental cement. Biomaterials 1995; 16(2):149-54.

[21] Till Vallée, João R. Correia, Thomas Keller. Optimum thickness of joints made of GFPR pultruded adherends and polyurethane adhesive. Compos Struct 2010;92(9):2102–8.

[22] Suzuki Y. Adhesive tensile strengths of scarf and butt joints of steel plates (Relation between adhesive layer thicknesses and adhesive strengths of joints). JSME IntJ 1987;30(265):1042–51.

[23] Zhang Y, Noda NA, Takaishi K, Lan X. Effect of adhesive thickness on the intensity of singular stress at the adhesive dissimilar joint. J Solid Mech Mater Eng 2010;4(10):1467–79.

[24] Noda NA, Zhang Y, Lan X, Takase Y, Oda K. Stress intensity factors of an interface crack in a bonded plate under uni-axial tension. J Solid Mech Mater Eng 2010;4(7):974–87.

[25] Lan X, Noda NA, Michinaka K, Zhang Y. The effect of material combinations and relative crack size on the stress intensity factors at the crack tip of a bi-material bonded strip. Eng Fract Mech 2011;78(14):2572–84.

[26] Noda NA, Lan X. Stress intensity factors for an edge interface crack in a bonded semi-infinite plate for arbitrary material combination. Int J Solids Struct 2012;49(10):1241–51.

[27] Zhang Y, Noda NA, Takaishi K, Lan X. Stress intensity factors of a central interface crack in a bonded finite plate and periodic interface cracks under arbitrary material combinations. Eng Fract Mech 2011;78(6):1218–32.

[28] Zhang Y. Intensity of singular stress field at the end of interface under arbitrary material combination. Japan: Kyushu Institute of Technology; 2011 Ph.D. dissertation.

[29] Zhang Y, Noda NA, Wu PZ, Duan ML. A mesh-independent technique to evaluate stress singularities in adhesive joints. Int J Adhes Adhes 2015;57:105– 17 the corrigendum of authorship is published in Int J Adhes Adhes 60, 2015.

[30] Noda NA, Oda K. Interaction effect of stress intensity factors for any number of collinear interface cracks. Int J Fract 1997;84:117–28.

[31] Bogy DB. Edge-bonded dissimilar orthogonal elastic wedges under normal and shear loading. Trans ASME J Appl Mech 1968;35(3):460–6.

[32] Bogy DB. Two edge-bonded elastic wedges of different materials and wedge angles under surface tractions. Trans ASME J Appl Mech 1971;38(2):377–86.

[33] Noda NA, Shirao R, Li J, Sugimoto JS. Intensity of singular stress fields causing interfacial debonding at the end of a fiber under pullout force and transverse tension. Int J Solids Struct 2007;44:4472–91.

[34] Inoue S. Mechanics of adhesion. Kobunshi 1956; 5(12):583–7. [in Japanese]

[35] Akisanya AR, Meng CS. Initiation of fracture at the interface corner of bi-material joints. J Mech Phys Solids 2003;51(1):27–46.

[36] Qian Z, Akisanya AR. An experimental investigation of failure initiation in bonded joints. Acta Mater 1998;46(14):4895–904.

[37] Mintzas A, Nowell D. Validation of an H_{cr}-based fracture initiation criterion for adhesively bonded joints. Eng Fract Mech 2012;80:13–27.

[38] Chen DH, Nisitani H. Singular stress fields near a corner of jointed dissimilar materials. Trans Jpn Soc Mech Eng A 1991;57(542):2509–15 [inJapanese].

[39] Chen DH, Noda NA, Takase Y, Morodomi T. Evaluation of static strength by the application of stress intensity of angular corner. Trans Jpn Soc Mech Eng A 1996;62(598):1445–9 [inJapanese].

[40] Chen DH, Noda NA. A consideration on the fracture criterion for a sharp notch. Trans Jpn Soc Mech Eng A 1998;64(626):2574–82 [inJapanese].

[41] Shimoda Y, Oda K, Tsutsumi N. Evaluation of singular field for V-shaped notch specimen by small crack concept. In: Proceedings of ACMFMS 2014 mechanics of functional materials and structures; 2014. p. 593–4.

[42] Oda K, Kamisugi K, Noda NA. Analysis of stress intensity factor for interface cracks based on proportional method. Trans Jpn Soc Mech Eng A 2009;75 (752):476–82 [inJapanese].

[43] Oda K, Noda NA, Atluri SN. Accurate determination of stress intensity factor for interface crack by finite element method. Key Eng Mater 2007;353- 358:3124–7.

[44] Terasaki T, Akiyama T, Kaneko T, Hisada H. Proposal of implant type torsion test for estimating adhesive strength of sprayed coatings. Q J Jpn Weld Soc 1991;9(4):97–103 [inJapanese].

[45]Terasaki T, Akiyama T, Kamiwaki S. Study of interfacial strength of bonded dissimilar materials. Q J Jpn Weld Soc 1992;10(2):83–8 [inJapanese].

[46]Chen DH, Nisitani H. Stress intensity factors K_{I,λ_1} and K_{II,λ_2} of a strip with a V-Shaped single notch under tension or in-plane bending. Trans Jpn Soc Mech Eng A 1993;59(560):1069–74 [inJapanese].

[47]Chen DH, Nisitani H. Singular stress fields near the tip of a V-notch in a semi-finite plate. Trans Jpn Soc Mech Eng A 1991;57(538):1406–11.

[48]Noda NA, Oda K, Inoue T. Analysis of newly-defined stress intensity factors for angular corners using singular integral equations of the body force method. Int J Fract 1996;76:243–61.

[49]Chen DH. Stress intensity factors for V-notched strip under tension or in-plane bending. Int J Fract 1995;70:81–97.

[50]Noda NA, Takase Y. Generalized stress intensity factors of V-shaped notch in a round bar under torsion, tension, and bending. Eng Fract Mech 2003;70:1447– 66.

Tables:

Table 1

Material properties of adherent and adhesives.

	Combination		Young's modulus E [GPa]	Poisson's ratio v	ε	α	β	λ
A	Adherent	Medium carbon steel S35C	210	0.30	-0.0641	0.969	0.199	0.685
	Adhesive	Epoxy resin A	3.14	0.37				
B	Adherent	Medium carbon steel S35C	210	0.30	-0.0607	0.978	0.188	0.674
	Adhesive	Epoxy resin B	2.16	0.38				

Table 2

Stress distributions for bonded strip under tension shown in Fig. 2 obtained by different mesh size when $h/W = 0.001$.

	Smallest mesh size $e_{\min} = 1/3^8$ around the edge			Smallest mesh size $e_{\min} = 1/3^4$ around the edge	
r/W	$\sigma_y^{FEM}\big|_{h/W=0.001}$	$\dfrac{\sigma_y^{FEM}\big|_{h/W=0.001}}{\sigma_{y*}^{FEM}}$	r/W	$\sigma_y^{FEM}\big|_{h/W=0.001}$	$\dfrac{\sigma_y^{FEM}\big|_{h/W=0.001}}{\sigma_{y*}^{FEM}}$
0	1.414	0.525	0	1.072	0.524
$1/6561000$	1.177	0.525	$1/81000$	0.889	0.522
$2/6561000$	1.138	0.525	$2/81000$	0.859	0.522
$3/6561000$	1.109	0.525	$3/81000$	0.838	0.522
$4/6561000$	1.088	0.525	$4/81000$	0.824	0.523
$5/6561000$	1.071	0.525	$5/81000$	0.813	0.525

Table 3

The experimentally obtained adhesive strength in Fig.1(a) expressed by $\sigma_y^\infty = \sigma_c$.

h [mm]	h/W	Medium carbon steel S35C, Epoxy resin A						Medium carbon steel S35C, Epoxy resin B			
		Measured values [MPa]					Average ± SD [MPa]	Measured values [MPa]			Average ± SD [MPa]
0.05	0.00394	47.7	50.0	58.4	63.5	66.5	57.2 ± 7.34	72.8	77.6	79.9	76.8 ± 2.96
0.1	0.00787	44.3	49.8	52.0	57.0	63.5	53.3 ± 6.52	70.2	71.5	72.6	71.4 ± 0.981
0.3	0.0236	28.6	30.8	32.5	34.2	36.5	32.5 ± 2.72	45.5	50.9	52.6	49.7 ± 3.03
0.6	0.0472	21.9	24.8	25.2	28.2	29.6	25.9 ± 2.71	39.6	40.0	43.9	41.2 ± 1.94
1.0	0.0787	21.5	21.5	21.9	23.5	24.4	22.6 ± 1.18	21.1	26.5	28.4	25.3 ± 3.09
2.0	0.157	14.8	18.1	18.2	19.9	20.9	18.4 ± 2.08	18.1	19.7	21.3	19.7 ± 1.31
5.0	0.394	11.4	11.4	13.6	15.0	15.6	13.4 ± 1.76	12.4	12.4	16.0	13.6 ± 1.70

SD : Standard deviation

Table 4

Adhesive strength σ_c and critical value of corner stress intensity factor $K_{\sigma c} = F_\sigma \sigma_c W^{1-\lambda}$ assuming perfectly bonded model.

h/W	Medium carbon steel S35C, Epoxy resin A			Medium carbon steel S35C, Epoxy resin B		
	σ_c [MPa]	F_σ	$K_{\sigma c}$ [MPa.m$^{0.315}$]	σ_c [MPa]	F_σ	$K_{\sigma c}$ [MPa.m$^{0.326}$]
0.001	–	0.0435	–	–	0.0396	–
0.00394	57.2	0.0671	0.970 ± 0.125	76.8	0.0620	1.15 ± 0.0442
0.00787	53.3	0.0831	1.12 ± 0.137	71.4	0.0778	1.34 ± 0.0184
0.01	–	0.0902	–	–	0.0842	–
0.0236	32.5	0.119	0.978 ± 0.0818	49.7	0.112	1.34 ± 0.0818
0.0472	25.9	0.150	0.981 ± 0.102	41.2	0.142	1.41 ± 0.0665
0.0787	22.6	0.178	1.02 ± 0.0532	25.3	0.171	1.04 ± 0.127
0.1	–	0.194	–	–	0.187	–
0.157	18.4	0.231	1.07 ± 0.121	19.7	0.223	1.06 ± 0.0703
0.394	13.4	0.335	1.13 ± 0.149	13.6	0.331	1.09 ± 0.135
0.5	–	0.363	–	–	0.360	–
$K_{\sigma c(average)}$	–	–	1.04 ± 0.0643	–	–	1.20 ± 0.144

Table 5

Material properties of adherent and adhesives.

	Combination		Young's modulus E [GPa]	Poisson's ratio v	ε	α	β	λ
C	Adherent	Aluminum	70	0.35	-0.0664	0.94	0.21	0.714
	Adhesive	Araldite	2.1	0.36				
D	Adherent	Brass	90	0.34	-0.0485	0.86	0.15	0.745
	Adhesive	Solder	6.4	0.39				

Table 6

Adhesive strength σ_c and critical value of corner stress intensity factor $K_{\sigma c} = F_\sigma \sigma_c W^{1-\lambda}$ assuming perfectly bonded model.

h [mm]	Aluminum, Araldite			Brass, Solder		
	σ_c [MPa]	F_σ	$K_{\sigma c}$ [MPa$\cdot$m$^{0.286}$]	σ_c [MPa]	F_σ	$K_{\sigma c}$ [MPa$\cdot$m$^{0.255}$]
0.5	12.4	0.173	0.574	90.3	0.186	5.18
1.0	10.2	0.217	0.593	68.9	0.230	4.89
1.5	8.61	0.250	0.577	57.3	0.263	4.66
2.5	8.49	0.303	0.690	47.2	0.320	4.66
3.0	7.03	0.325	0.612	43.2	0.345	4.60
$K_{\sigma c(average)}$	–	–	0.609±0.0475	–	–	4.80±0.780

Table 7

Results of notch stress intensity factor K_{IC,λ_1} and

singularity index λ_1

γ	$K_{IC,\lambda_1}\,[\text{N/mm}^{1+\lambda_1}]$	λ_1
$30°$	38.0 ± 1.2	0.50145
$60°$	40.2 ± 2.4	0.51222
$90°$	42.9 ± 1.6	0.54448

Table 8

Dimensionless stress intensity factor F_I and

singularity index γ for $a/t \leq 0.005$

γ	F_I	λ_1
15°	0.995	0.50018
30°	0.985	0.50145
60°	0.961	0.51222
90°	0.953	0.54448

Table 9

Adhesive strength σ_c and critical value of interface stress intensity factor K_{IC} assuming fictitious crack model when $a/W = 0.01, 0.1$.

(a) Medium carbon steel S35C, Epoxy resin A

h/W	σ_c [MPa]	$a/W = 0.01$			$a/W = 0.1$		
		F_I	F_{II}/F_I	K_{IC} [MPa$\sqrt{\text{m}}$]	F_I	F_{II}/F_I	K_{IC} [MPa$\sqrt{\text{m}}$]
0.001	–	0.256	-0.507	–	0.214	-0.703	–
0.00394	57.2	0.367	-0.418	0.419 ± 0.0538	0.237	-0.577	0.856 ± 0.110
0.00787	53.3	0.457	-0.415	0.487 ± 0.0596	0.271	-0.521	0.914 ± 0.112
0.01	–	0.492	-0.424	–	0.288	-0.504	–
0.0236	32.5	0.631	-0.446	0.410 ± 0.0343	0.372	-0.446	0.765 ± 0.0640
0.0472	25.9	0.790	-0.430	0.409 ± 0.0427	0.478	-0.416	0.783 ± 0.0818
0.0787	22.6	0.952	-0.407	0.429 ± 0.0224	0.579	-0.418	0.825 ± 0.0431
0.1	–	1.04	-0.397	–	0.633	-0.425	–
0.157	18.4	1.26	-0.379	0.463 ± 0.0524	0.744	-0.434	0.863 ± 0.0976
0.394	13.4	1.88	-0.356	0.503 ± 0.0660	1.06	-0.400	0.899 ± 0.118
0.5	–	1.94	-0.353	–	1.15	-0.382	–
$K_{IC(average)}$	–	–	–	0.446 ± 0.0356	–	–	0.844 ± 0.0517

(σ_c : Experimental result, $K_{IC} = F_I \, \sigma_c \, \sqrt{\pi a}$)

(b) Medium carbon steel S35C, Epoxy resin B

h/W	σ_c [MPa]	$a/W = 0.01$			$a/W = 0.1$		
		F_I	F_{II}/F_I	K_{IC} [MPa$\sqrt{\text{m}}$]	F_I	F_{II}/F_I	K_{IC} [MPa$\sqrt{\text{m}}$]
0.001	–	0.228	-0.509	–	0.183	-0.699	–
0.00394	76.8	0.340	-0.423	0.521 ± 0.0201	0.208	-0.577	1.010 ± 0.0389
0.00787	71.4	0.431	-0.425	0.615 ± 0.00844	0.244	-0.523	1.100 ± 0.0151
0.01	–	0.466	-0.436	–	0.261	-0.506	–
0.0236	49.7	0.604	-0.464	0.599 ± 0.0365	0.347	-0.450	1.089 ± 0.0664
0.0472	41.2	0.767	-0.442	0.631 ± 0.0297	0.455	-0.423	1.182 ± 0.0557
0.0787	25.3	0.936	-0.415	0.474 ± 0.0578	0.557	-0.429	0.891 ± 0.109
0.1	–	1.04	-0.402	–	0.611	-0.438	–
0.157	19.7	1.26	-0.382	0.466 ± 0.0330	0.723	-0.450	0.900 ± 0.0597
0.394	13.6	1.93	-0.357	0.500 ± 0.0653	1.06	-0.409	0.908 ± 0.113
0.5	–	1.99	-0.353	–	1.15	-0.389	–
$K_{IC(average)}$	–	–	–	0.551 ± 0.0576	–	–	1.01 ± 0.107

(σ_c : Experimental result, $K_{IC} = F_I \, \sigma_c \, \sqrt{\pi a}$)

Table 10

Adhesive strength σ_c and critical value of interface stress intensity factor K_{IC} assuming fictitious crack model when $a/W = 0.01, 0.1$.

(a) Aluminum, Araldite

h [mm]	σ_c [MPa]	$a/W = 0.01$			$a/W = 0.1$		
		F_I	F_{II}/F_I	K_{IC} [MPa$\sqrt{m}$]	F_I	F_{II}/F_I	K_{IC} [MPa$\sqrt{m}$]
0.5	12.4	0.823	0.413	0.180	0.530	0.400	0.367
1.0	10.2	1.042	0.386	0.188	0.663	0.406	0.379
1.5	8.61	1.210	0.372	0.185	0.754	0.413	0.364
2.5	8.49	1.483	0.359	0.223	0.898	0.407	0.427
3.0	7.03	1.598	0.355	0.199	0.959	0.400	0.378
$K_{IC(average)}$	–	–	–	0.195 ± 0.015	–	–	0.383 ± 0.023

(σ_c : Experimental result, $K_{IC} = F_I \sigma_c \sqrt{\pi a}$)

(b) Brass, Solder

h [mm]	σ_c [MPa]	$a/W = 0.01$			$a/W = 0.1$		
		F_I	F_{II}/F_I	K_{IC} [MPa$\sqrt{m}$]	F_I	F_{II}/F_I	K_{IC} [MPa$\sqrt{m}$]
0.5	90.3	0.799	0.394	1.279	0.601	0.353	3.044
1.0	68.9	0.994	0.360	1.213	0.695	0.380	2.686
1.5	57.3	1.149	0.344	1.166	0.764	0.396	2.454
2.5	47.2	1.412	0.328	1.180	0.893	0.391	2.360
3.0	43.2	1.527	0.324	1.168	0.953	0.382	2.307
$K_{IC(average)}$	–	–	–	1.201 ± 0.042	–	–	2.570 ± 0.270

(σ_c : Experimental result, $K_{IC} = F_I \sigma_c \sqrt{\pi a}$)

Table 11

F_I and C_I values in Fig. 1(c).

(a) Medium carbon steel S35C, Epoxy resin A

a/W	$h/W = 0.0472$		$h/W = 0.0787$		$h/W = 0.1$		$h/W = 0.157$		$h/W = 0.394$		$h/W = 0.5$		$h/W \geq 1$	
	F_I	C_I	F_I	C_I	F_I	C_I	F_I	C_I	F_I	C_I	F_I	C_I	F_I	C_I
0.0001	3.640	0.2000	4.341	0.2386	4.729	0.2599	5.611	0.3083	8.155	0.4482	8.838	0.4857	9.838	0.5406
0.001	1.724	0.1957	2.073	0.2353	2.265	0.2571	2.699	0.3063	3.938	0.4470	4.269	0.4845	4.753	0.5394
0.002	1.363	0.1925	1.648	0.2327	1.804	0.2547	2.156	0.3044	3.159	0.4460	3.426	0.4838	3.818	0.5391
0.005	0.9932	0.1872	1.205	0.2271	1.323	0.2493	1.596	0.3008	2.355	0.4437	2.559	0.4821	2.861	0.5391
0.01	0.7897	0.1851	0.9520	0.2232	1.048	0.2457	1.262	0.2958	1.880	0.4406	2.054	0.4816	2.309	0.5413
0.05	0.5301	0.2063	0.6251	0.2433	0.6764	0.2633	0.8000	0.3114	1.170	0.4554	1.279	0.4979	1.489	0.5718
0.1	0.4780	0.2314	0.5792	0.2804	0.6331	0.3065	0.7435	0.3600	1.062	0.5140	1.154	0.5585	1.320	0.6391
0.2	0.5049	0.3041	0.6209	0.3740	0.6856	0.4129	0.8272	0.4982	1.157	0.6968	1.241	0.7477	1.387	0.8354

(b) Medium carbon steel S35C, Epoxy resin B

a/W	$h/W = 0.0472$		$h/W = 0.0787$		$h/W = 0.1$		$h/W = 0.157$		$h/W = 0.394$		$h/W = 0.5$		$h/W \geq 1$	
	F_I	C_I	F_I	C_I	F_I	C_I	F_I	C_I	F_I	C_I	F_I	C_I	F_I	C_I
0.0001	3.779	0.1877	4.539	0.2254	4.962	0.2464	5.936	0.2948	8.797	0.4369	9.569	0.4752	10.70	0.5314
0.001	1.743	0.1834	2.113	0.2222	2.317	0.2437	2.784	0.2929	4.143	0.4358	4.507	0.4742	5.040	0.5302
0.002	1.365	0.1800	1.665	0.2196	1.830	0.2414	2.207	0.2910	3.298	0.4349	3.591	0.4735	4.018	0.5299
0.005	0.9784	0.1739	1.201	0.2134	1.327	0.2358	1.616	0.2872	2.434	0.4326	2.654	0.4718	2.981	0.5300
0.01	0.7671	0.1709	0.9364	0.2087	1.038	0.2312	1.264	0.2816	1.927	0.4293	2.115	0.4712	2.388	0.5321
0.05	0.5063	0.1907	0.6015	0.2265	0.6543	0.2461	0.7809	0.2941	1.173	0.4418	1.290	0.4856	1.491	0.5616
0.1	0.4545	0.2146	0.5568	0.2628	0.6114	0.2886	0.7234	0.3415	1.057	0.4987	1.154	0.5448	1.330	0.6280
0.2	0.4794	0.2837	0.5974	0.3535	0.6632	0.3924	0.8078	0.4780	1.148	0.6796	1.237	0.7322	1.391	0.8230

Table 12

Results of estimated adhesive tensile strength σ_c.

(a) Medium carbon steel S35C, Epoxy resin A

h/W	Experimental adhesive strength σ_c [MPa]	Perfectly bonded model σ_c [MPa] when $K_{\sigma c}$ = 1.04 MPa·m$^{0.315}$ (Error %)	Fictitious crack model $a/W = 0.01$ σ_c [MPa] when K_{IC} = 0.446 MPa$\sqrt{m}$ (Error %)	Fictitious crack model $a/W = 0.1$ σ_c [MPa] when K_{IC} = 0.844 MPa$\sqrt{m}$ (Error %)
0.001	–	94.5	74.7	58.5
0.00392	57.2	61.3 (+7.1%)	60.9 (+6.4%)	56.4 (−1.4%)
0.00787	53.3	49.5 (−7.2%)	48.8 (−8.4%)	49.2 (−7.7%)
0.01	–	56.2	43.7	46.0
0.0236	32.5	34.5 (+6.2%)	35.4 (+8.8%)	35.9 (+10.3%)
0.0472	25.9	27.5 (+5.9%)	28.3 (+8.9%)	27.9 (+7.7%)
0.0787	22.6	23.0 (+2.1%)	23.4 (+3.9%)	23.1 (+2.2%)
0.1	–	19.5	21.4	21.3
0.157	18.4	17.8 (−3.0%)	17.7 (−3.8%)	18.0 (−2.3%)
0.394	13.4	12.3 (−8.5%)	11.9 (−11.4%)	12.6 (−6.1%)
0.5	–	11.3	14.5	14.1

(b) Medium carbon steel S35C, Epoxy resin B

h/W	Experimental adhesive strength σ_c [MPa]	Perfectly bonded model σ_c [MPa] when $K_{\sigma c}$ = 1.20 MPa·m$^{0.326}$ (Error %)	Fictitious crack model $a/W = 0.01$ σ_c [MPa] when K_{IC} = 0.551 MPa$\sqrt{m}$ (Error %)	Fictitious crack model $a/W = 0.1$ σ_c [MPa] when K_{IC} = 1.01 MPa$\sqrt{m}$ (Error %)
0.001	–	98.3	118.0	84.0
0.00392	76.8	80.6 (+5.0%)	81.2 (+5.8%)	76.9 (+0.1%)
0.00787	71.4	64.2 (−10.1%)	64.1 (−10.3%)	65.7 (−8.1%)
0.01	–	76.4	58.0	61.2
0.0236	49.7	44.5 (−10.3%)	45.7 (−8.0%)	46.1 (−7.1%)
0.0472	41.2	35.1 (−14.7%)	36.0 (−12.6%)	35.2 (−14.4%)
0.079	25.3	29.3 (+15.5%)	29.5 (+16.4%)	28.8 (+13.5%)
0.1	–	23.4	25.9	25.9
0.157	19.7	22.4 (+13.5%)	21.8 (+10.9%)	22.1 (+12.4%)
0.394	13.4	15.1 (+11.0%)	14.3 (+5.4%)	15.2 (+11.4%)

0.5	–	17.4	12.9	14.1

Table A.1 $F_\sigma\big|_{h/W=1}$ at interface edge point in bonded finite plate

[underlined figures indicate $\lambda<1$, **bold** figures indicate $\lambda>1$, standard style figures indicate $\lambda=1$]

α	$\beta=-0.4$	$\beta=-0.3$	$\beta=-0.2$	$\beta=-0.1$	$\beta=0$	$\beta=0.1$	$\beta=0.2$	$\beta=0.3$	$\beta=0.4$
1.0	0.540	0.446	0.395	0.357	0.332				
-0.95	0.643	0.491	0.422	0.381	0.349				
-0.9	0.726	0.534	0.456	0.412	0.381				
-0.8	1.000	0.636	0.538	0.487	0.45				
-0.7	**1.855**	0.800	0.626	0.558	0.486				
-0.6	**3.291**	1.000	0.724	0.638	0.559	0.505			
-0.5		**1.264**	0.842	0.722	0.635	0.551			
-0.4		**1.467**	1.000	0.822	0.718	0.615			
-0.3		**1.609**	**1.118**	0.913	0.796	0.697			
-0.2		**1.690**	**1.153**	1.000	0.889	0.797	0.404		
-0.1			**1.103**	**1.037**	0.955	0.890	0.767		
0			1.000	1.000	1.000	1.000	1.000		
0.1			0.767	0.890	0.955	**1.037**	**1.103**		
0.2			0.404	0.797	0.889	1.000	**1.153**	**1.690**	
0.3				0.697	0.796	0.913	**1.118**	**1.609**	
0.4				0.615	0.718	0.822	1.000	**1.467**	
0.5				0.551	0.635	0.722	0.842	**1.264**	
0.6				0.505	0.559	0.638	0.724	1.000	**3.291**
0.7					0.486	0.558	0.626	0.800	**1.855**
0.8					0.450	0.487	0.538	0.636	1.000
0.9					0.381	0.412	0.456	0.534	0.726
0.95					0.349	0.381	0.422	0.491	0.643
1.0					0.332	0.357	0.395	0.446	0.540

Table A.2

$F_\sigma / F_\sigma \mid_{h/W=1}$ with varying α and β when (a) $h/W = 0.001$; (b) $h/W = 0.1$.

(a) $h/W = 0.001$ (Note that $F_\sigma / F_\sigma \mid_{h/W=1} = 1$ when $\alpha = 2\beta$) [underlined figures indicate $\lambda < 1$, **bold** figures indicate $\lambda > 1$, standard style figures indicate $\lambda = 1$]

α	$\beta=-0.4$	$\beta=-0.3$	$\beta=-0.2$	$\beta=-0.1$	$\beta=0$	$\beta=0.1$	$\beta=0.2$	$\beta=0.3$	$\beta=0.4$
-1.0	0.682	0.566	0.517	0.552	0.400				
-0.95	0.6864	0.5554	0.4957	0.4629	0.400				
-0.9	0.7420	0.5533	0.4722	0.4252	0.4004				
-0.8	1.0000	0.6535	0.5254	0.4587	0.4190				
-0.7	**1.4465**	0.8130	0.6289	0.5356	0.4812				
-0.6	**2.073**	1.0000	0.7579	0.6390	0.5690	0.550			
-0.5		**1.1509**	0.8952	0.7587	0.6769	0.6297			
-0.4		**1.1613**	1.0000	0.8794	0.7988	0.7530			
-0.3		**1.0165**	1.0232	0.9725	0.9205	0.8924			
-0.2		**0.750**	0.9346	1.0000	1.0169	1.0203	1.100		
-0.1			**0.7716**	0.9372	1.0526	1.1374	1.280		
0			0.5912	0.7994	1.0000	1.1925	1.3925		
0.1			0.4363	0.6331	0.8665	**1.1473**	**1.4837**		
0.2			0.300	0.4768	0.6938	1.0000	**1.4608**	2.524	
0.3				0.3477	0.5253	0.7974	**1.2786**	2.443	
0.4				0.2478	0.3834	0.5962	1.0000	2.0311	
0.5				0.1728	0.2729	0.4281	0.7223	**1.5100**	
0.6				0.150	0.1904	0.2996	0.4984	1.0000	**2.857**
0.7					0.1297	0.2058	0.3355	0.6323	**1.825**
0.8					0.0852	0.1388	0.2224	0.3942	1.0000
0.9					0.0511	0.0913	0.1456	0.2448	0.5173
0.95					0.0348	0.0725	0.1172	0.1930	0.3806
1.0					0.025	0.050	0.080	0.110	0.300

(b) $h/W = 0.1$ (Note that $F_\sigma / F_\sigma \mid_{h/W=1} = 1$ when $\alpha = 2\beta$) [underlined figures indicate $\lambda < 1$, **bold** figures indicate $\lambda > 1$, standard style figures indicate $\lambda = 1$]

α	$\beta=-0.4$	$\beta=-0.3$	$\beta=-0.2$	$\beta=-0.1$	$\beta=0$	$\beta=0.1$	$\beta=0.2$	$\beta=0.3$	$\beta=0.4$
-1	1.000	1.000	1.000	1.000	1.000				
-0.95	1.0099	1.0143	1.0164	1.0177	1.018				
-0.9	1.0144	1.0260	1.0312	1.0342	1.0365				
-0.8	1.0000	1.0390	1.0548	1.0637	1.0698				
-0.7	**0.9275**	1.0333	1.0681	1.0870	1.0993				
-0.6	**0.764**	1.0000	1.0671	1.1018	1.1239	1.150			
-0.5		**0.9298**	1.0462	1.1048	1.1415	1.1686			
-0.4		**0.8228**	1.0000	1.0916	1.1491	1.1910			

-0.3	**0.6943**	**0.9269**	1.0575	1.1426	1.2051			
-0.2	**0.552**	**0.8345**	1.0000	1.1175	1.2051	1.260		
-0.1		**0.7361**	**0.9219**	1.0698	1.1890	1.280		
0		0.6433	0.8324	1.0000	1.1501	1.2864		
0.1		0.5579	0.7413	0.9144	**1.0856**	**1.2580**		
0.2		0.513	0.6548	0.8229	1.0000	**1.1994**	**1.453**	
0.3			0.5748	0.7332	0.9037	**1.1092**	**1.409**	
0.4			0.5007	0.6492	0.8071	1.0000	**1.2962**	
0.5			0.4307	0.5715	0.7160	0.8879	**1.1518**	
0.6			0.382	0.4994	0.6324	0.7828	1.0000	**1.498**
0.7				0.4309	0.5561	0.6882	0.8635	**1.224**
0.8				0.3625	0.4855	0.6040	0.7467	1.0000
0.9				0.2851	0.4180	0.5291	0.6479	0.8241
0.95				0.2329	0.3836	0.4947	0.6046	0.7544
1.0				0.185	0.339	0.463	0.560	0.697

Table B.1

Tabulated values of C_I.

α	$\beta = -0.2$	$\beta = -0.1$	$\beta = 0$	$\beta = 0.1$	$\beta = 0.2$	$\beta = 0.3$	$\beta = 0.4$	$\beta = 0.45$
0.05	1.036	1.082	1.114	1.136				
0.1	0.979	1.043	1.094	1.146	1.187			
0.15	0.907	1.001	1.063	1.14	1.221			
0.2		0.958	1.025	1.12	1.24			
0.3		0.875	0.938	1.044	1.215			
0.4		0.798	0.852	0.947	1.115	1.528		
0.5		0.721	0.772	0.85	0.986	1.343		
0.6			0.7	0.763	0.863	1.106		
0.7			0.635	0.686	0.756	0.912	1.876	
0.75			0.604	0.651	0.709	0.833	1.356	
0.8			0.573	0.618	0.666	0.764	1.092	
0.85			0.542	0.586	0.626	0.704	0.925	1.589
0.9			0.508	0.556	0.588	0.65	0.806	1.083
0.95			0.46	0.527	0.553	0.602	0.715	0.867

Table B.2

Tabulated values of C_{II}.

α	$\beta = -0.2$	$\beta = -0.1$	$\beta = 0$	$\beta = 0.1$	$\beta = 0.2$	$\beta = 0.3$	$\beta = 0.4$	$\beta = 0.45$
0.05	-0.083	-0.06	-0.026	0.014				
0.1	-0.093	-0.079	-0.052	-0.013	0.031			
0.15	-0.098	-0.094	-0.074	-0.041	0.006			
0.2		-0.106	-0.094	-0.067	-0.023			
0.3		-0.124	-0.123	-0.113	-0.084			
0.4		-0.133	-0.141	-0.144	-0.135	-0.095		
0.5		-0.137	-0.151	-0.162	-0.169	-0.166		
0.6			-0.156	-0.172	-0.187	-0.204		
0.7			-0.156	-0.176	-0.194	-0.218	-0.318	
0.75			-0.155	-0.176	-0.195	-0.219	-0.288	
0.8			-0.153	-0.175	-0.194	-0.219	-0.273	
0.85			-0.15	-0.173	-0.193	-0.217	-0.262	-0.379
0.9			-0.145	-0.171	-0.19	-0.214	-0.252	-0.307
0.95			-0.136	-0.168	-0.187	-0.209	-0.243	-0.278

Figures:

a   b   c
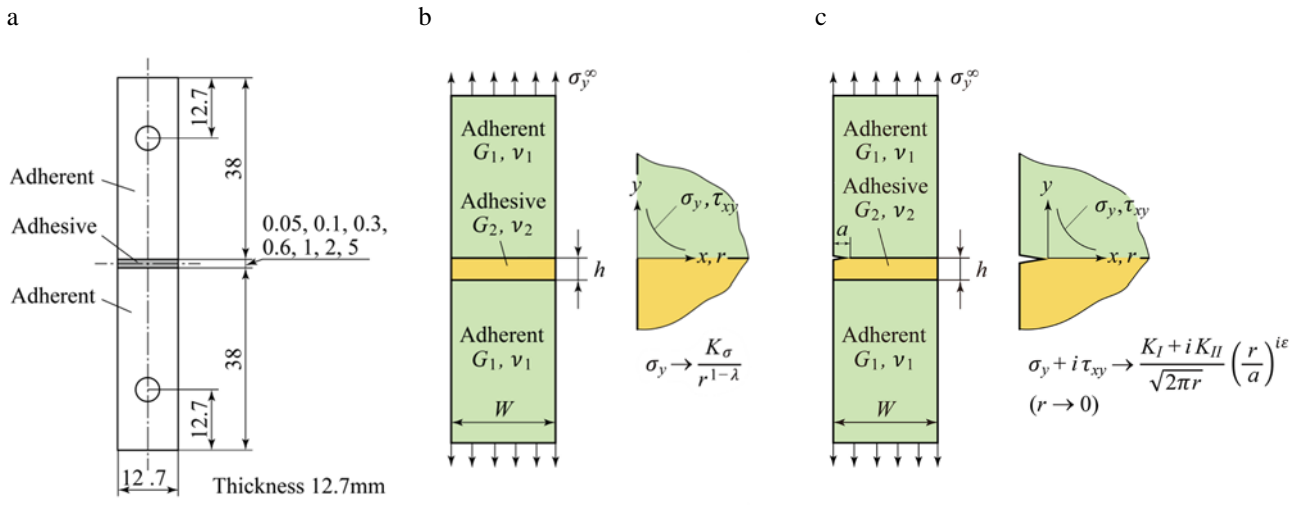
Fig. 1. Experimental specimen and two kinds of models used in this study. (a) Experimental specimen, (b) Perfectly-bonded model, (c) Fictitious crack model.
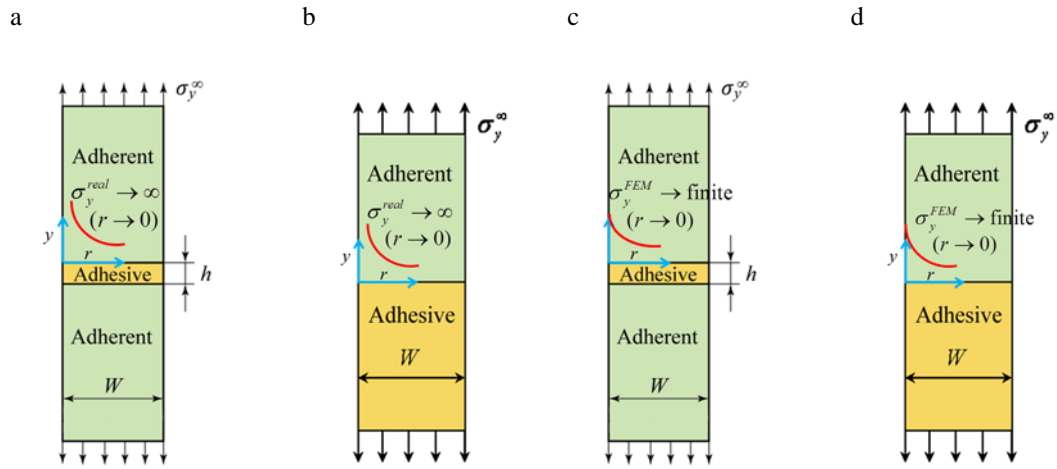
Fig. 2. Real stress σ_y^{real} for (a) $h/W = 0.001$, (b) $h/W \geq 1$ and

FEM stress σ_y^{FEM} for (c) $h/W = 0.001$, (d) $h/W \geq 1$.
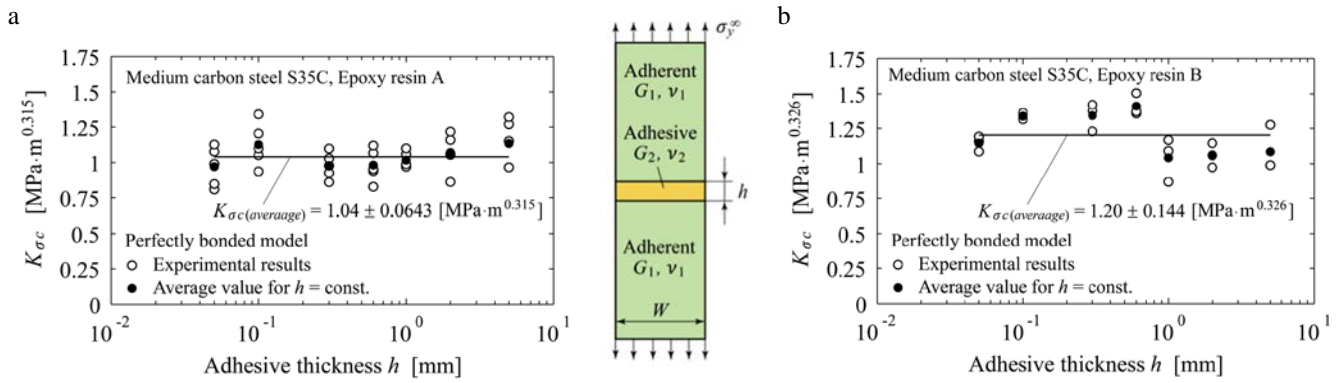
Fig.3. Adhesive strength for bonded Medium carbon steel S35C expressed as a constant critical value of corner stress

intensity factor $K_{\sigma c}$. (a) Medium carbon steel S35C, Epoxy resin A, (b) Medium carbon steel S35C, Epoxy resin B.

a
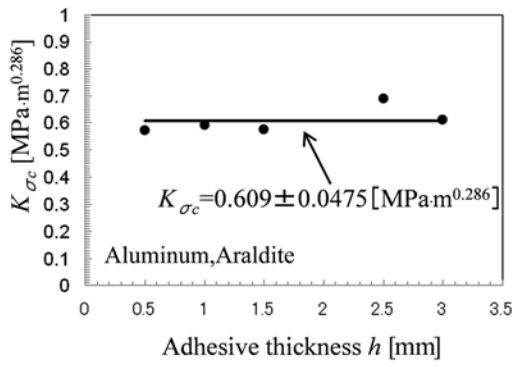
b
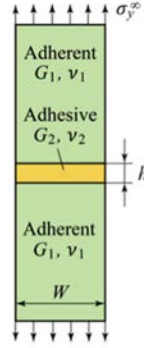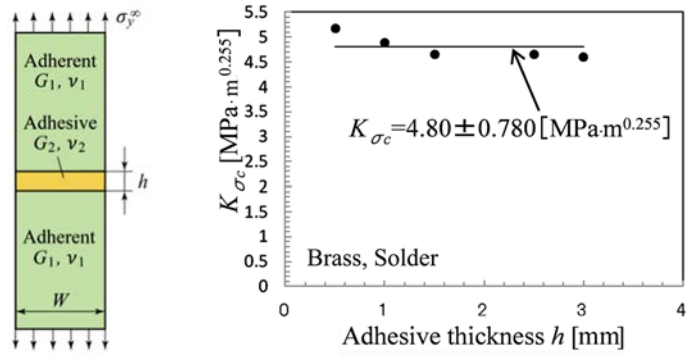
**Fig. 4.** Adhesive strength for bonded Aluminum and bonded Brass expressed as a constant critical value of corner stress intensity factor $K_{\sigma c}$. (a) Aluminum, Araldite, (b) Brass, Solder.
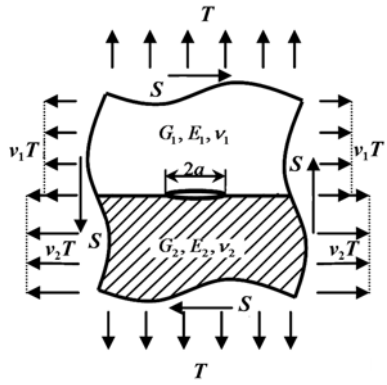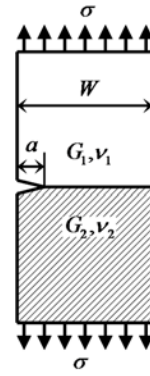
Fig. 5. (a) Reference problem A and (b) a given unknown problem B to explain the method of analysis.
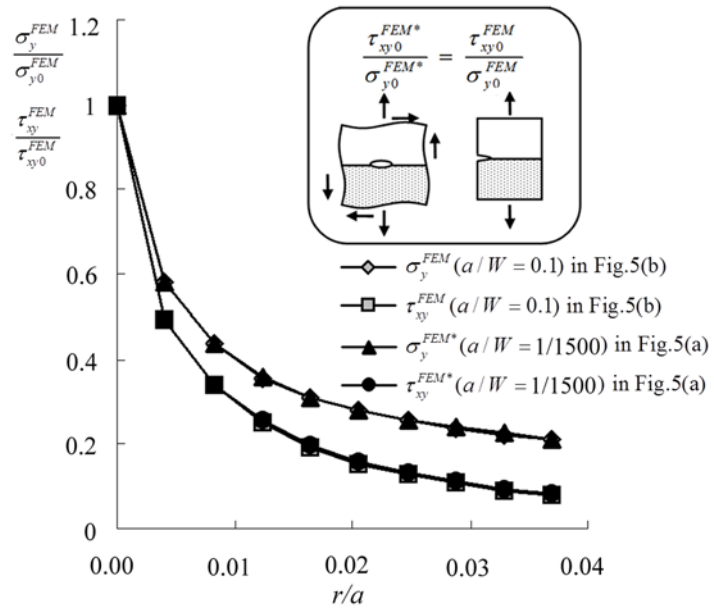
Fig.6. Comparison of relative stress distributions near crack tip.
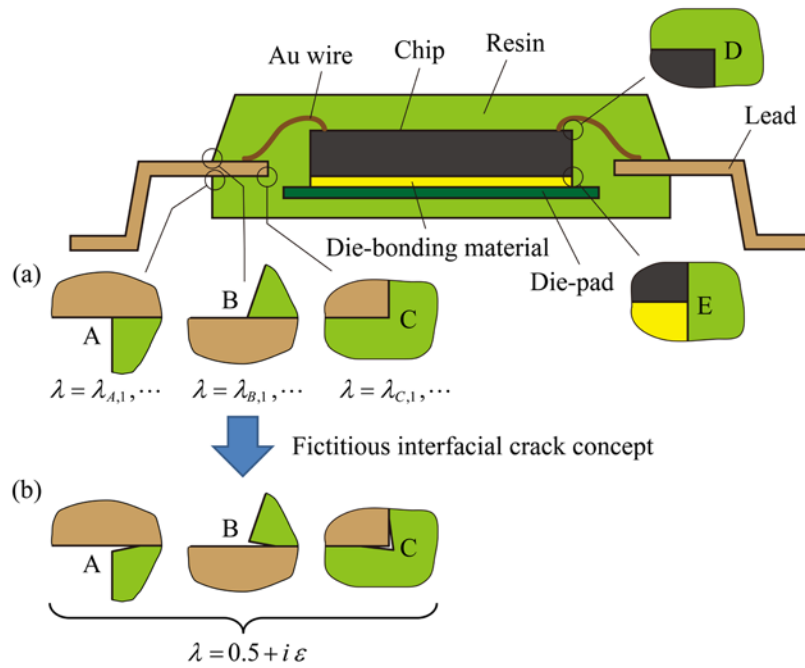
Fig. 7. An example of IC package; (a) perfectly bonded model; (b) fictitious crack model
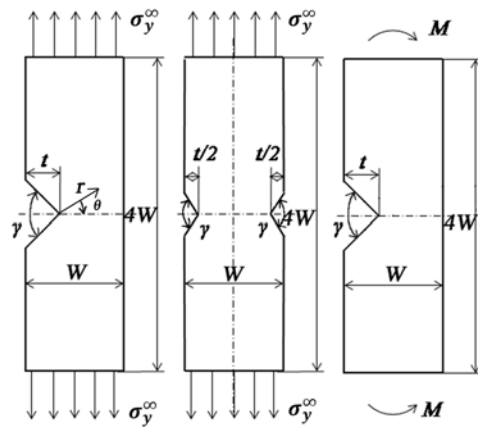
Fig.8. V-shaped sharp notch specimens of acrylic resin (W =40mm).
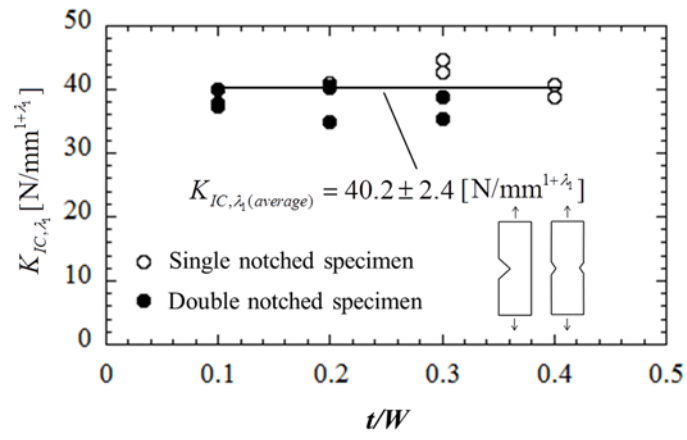
Fig. 9. Experimental results of critical value of notch stress intensity factor K_{IC,λ_1} for notches

of $\gamma = 60^o$ with various notch depths t.
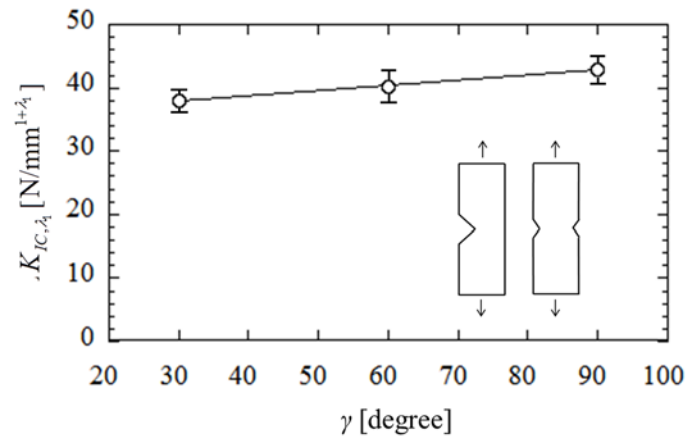
Fig. 10. Results of critical value of notch stress intensity factor K_{IC,λ_1} (average $\pm$ standard deviation).
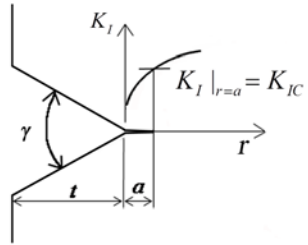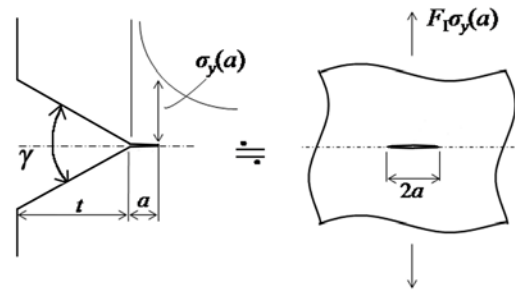
Fig.11. (a) Fracture criterion at notch root based on (b) the results for dimensionless stress intensity factor.
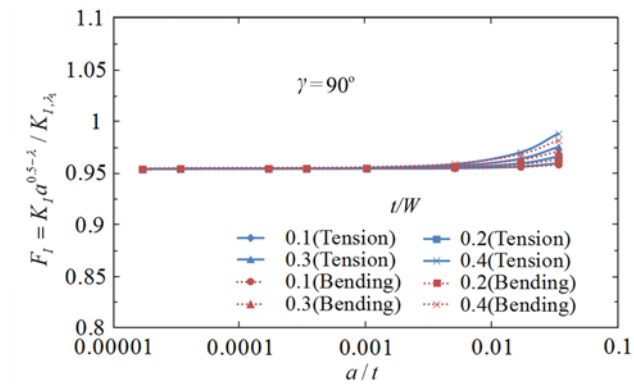
Fig.12. Relation between dimensionless stress intensity factor F_I and a/t when $\gamma = 90^o$.
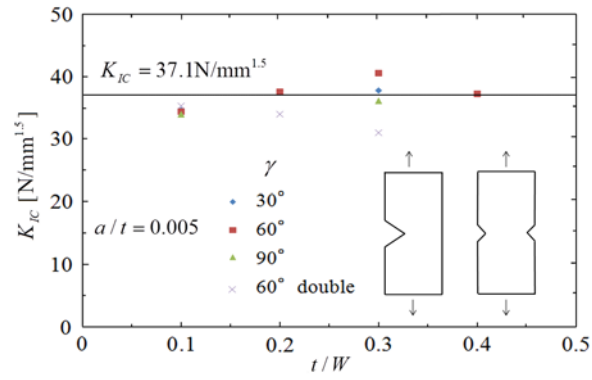
Fig.13. Static strength of acrylic resin with different V-shaped notches expressed as a constant critical

value of stress intensity factor K_{IC} by assuming fictitious crack $a/t = 0.005$ (a =0.02-0.08mm) in

Fig.11.
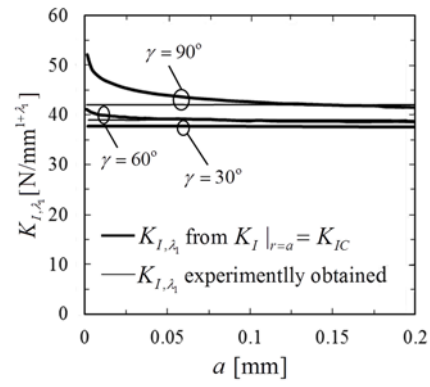
Fig. 14. Predicted K_{I,λ_1} based on $K_I|_{r=a} = K_{IC}$ in Fig. 11 and K_{I,λ_1} experimentally obtained.
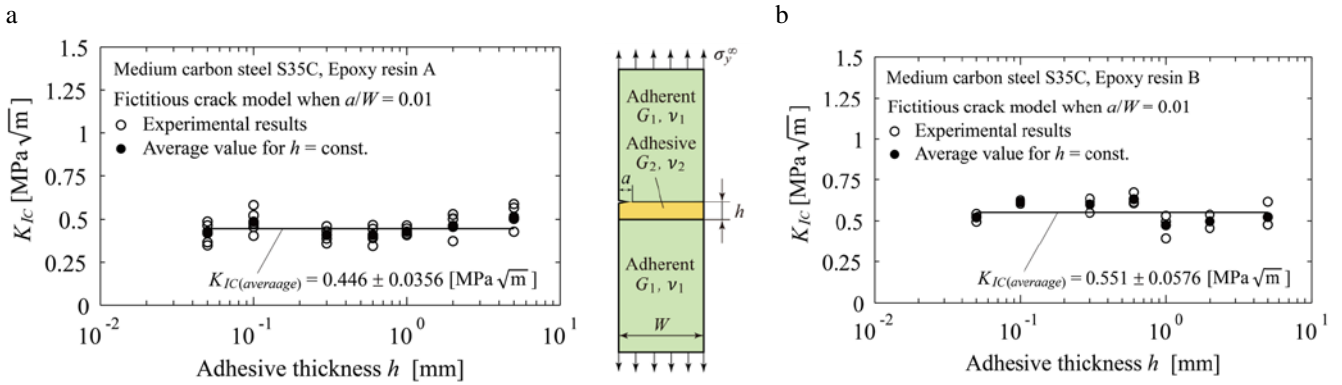
Fig.15. Adhesive strength for bonded Medium carbon steel S35C expressed as a constant critical value of interface stress intensity factor K_{IC} by assuming fictitious crack $a/W = 0.01$. (a) Medium carbon steel S35C, Epoxy resin A, (b) Medium carbon steel S35C, Epoxy resin B.
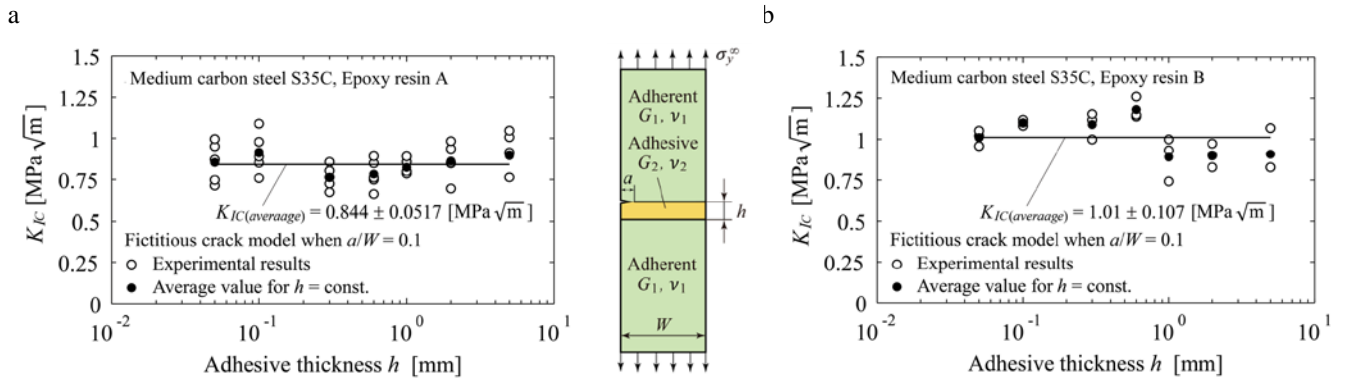
Fig.16. Adhesive strength for bonded Medium carbon steel S35C expressed as a constant critical value of interface stress intensity factor K_{IC} by assuming fictitious crack $a/W = 0.1$. (a) Medium carbon steel S35C, Epoxy resin A, (b) Medium carbon steel S35C, Epoxy resin B.

a

b
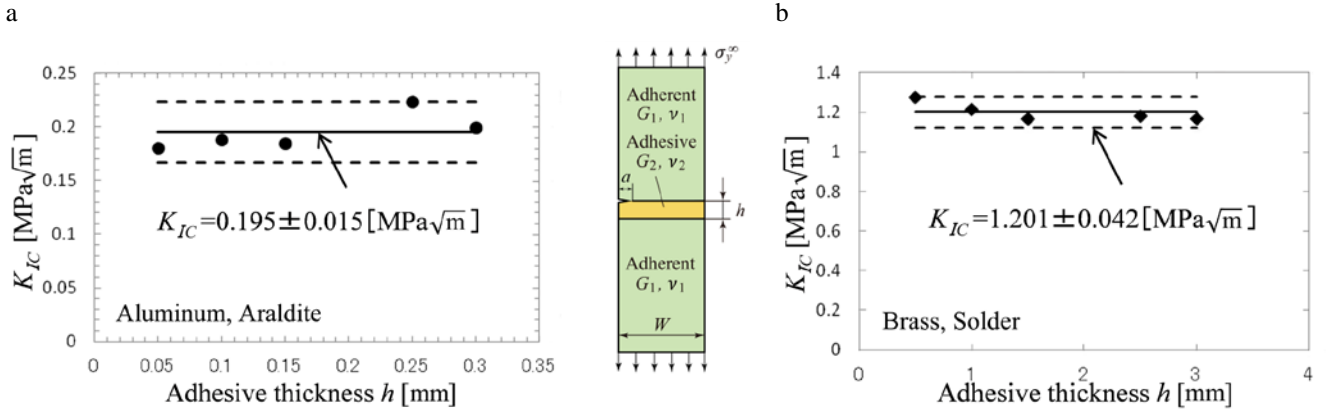
Fig.17. Adhesive strength for bonded Aluminum and bonded Brass expressed as a constant critical value of interface stress

intensity factor K_{IC} by assuming fictitious crack $a/W = 0.01$. (a) Aluminum, Araldite, (b) Brass, Solder.

a

b
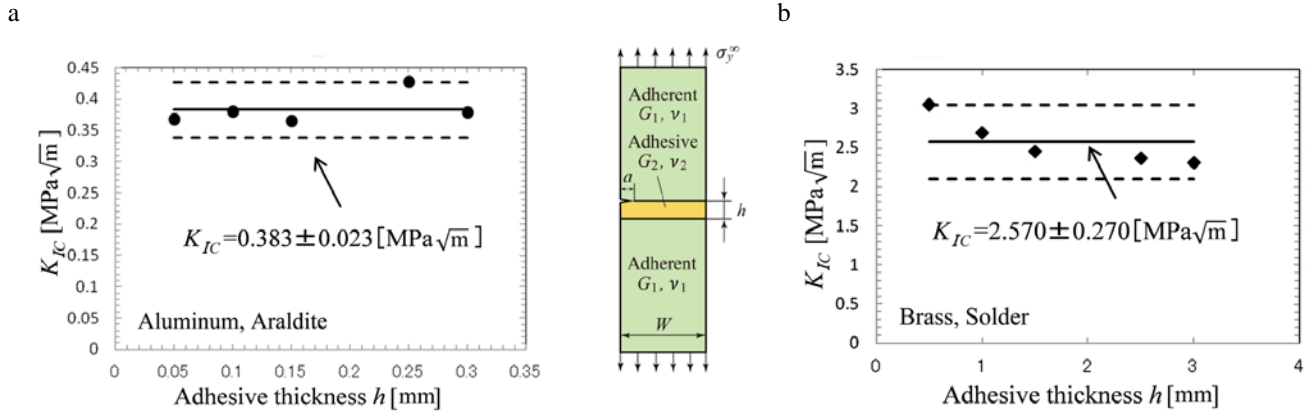
Fig. 18. Adhesive strength for bonded Aluminum and bonded Brass expressed as a constant critical value of interface stress

intensity factor K_{IC} by assuming fictitious crack $a/W = 0.1$. (a) Aluminum, Araldite, (b) Brass, Solder.
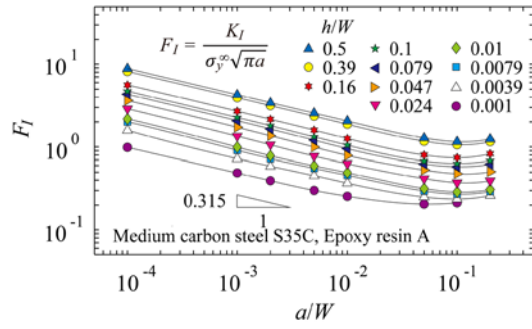
a   b
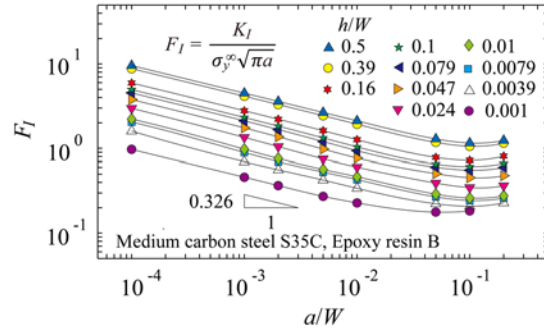
Fig. 19. Relationship between F_I and a/W for bonded Medium carbon steel S35C. (a) Medium carbon steel S35C, Epoxy resin A, (b) Medium carbon steel S35C, Epoxy resin B.
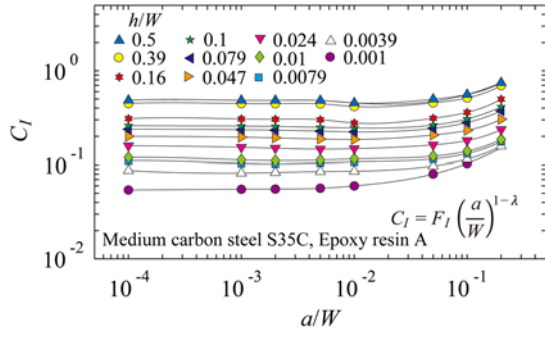
a b
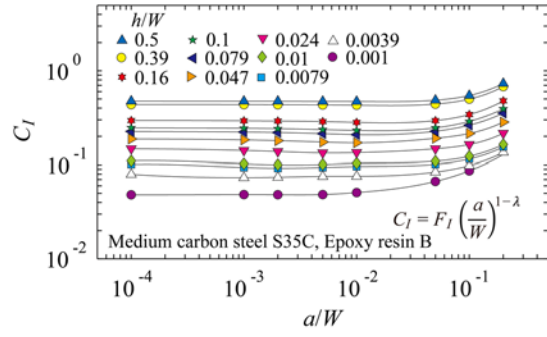
Fig. 20.   Relationship between C_I and a/W for bonded Medium carbon steel S35C. (a) Medium carbon
steel S35C, Epoxy resin A, (b) Medium carbon steel S35C, Epoxy resin B.
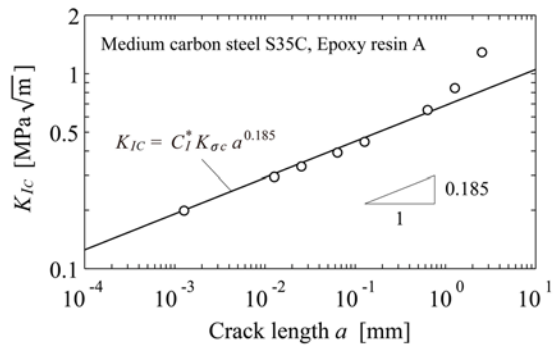
a
b
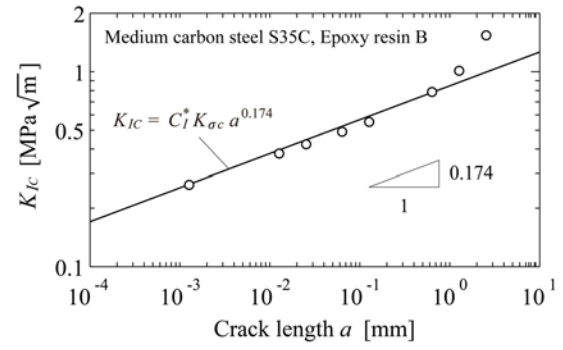
Fig. 21. Relationship between K_{IC} and "a" for bonded Medium carbon steel S35C. (a) Medium

carbon steel S35C, Epoxy resin A, (b) Medium carbon steel S35C, Epoxy resin B.

a
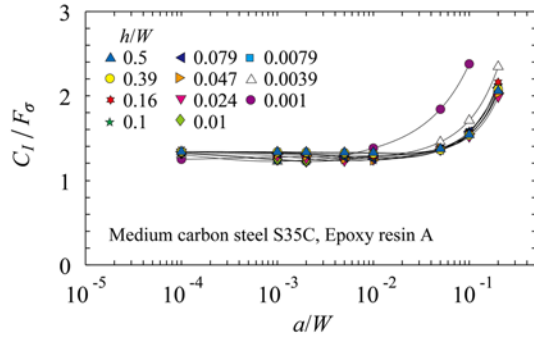
b
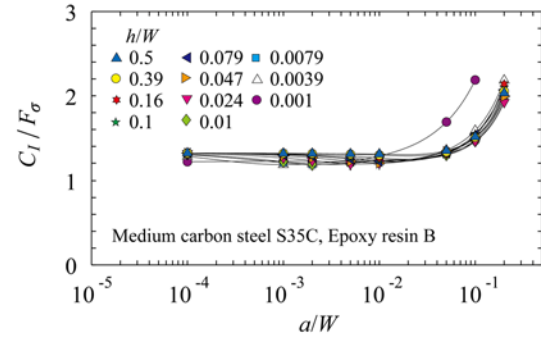
Fig. 22. Relationship between C_I/F_σ and a/W for bonded Medium carbon steel S35C. (a) Medium carbon steel S35C, Epoxy resin A, (b) Medium carbon steel S35C, Epoxy resin B.

a
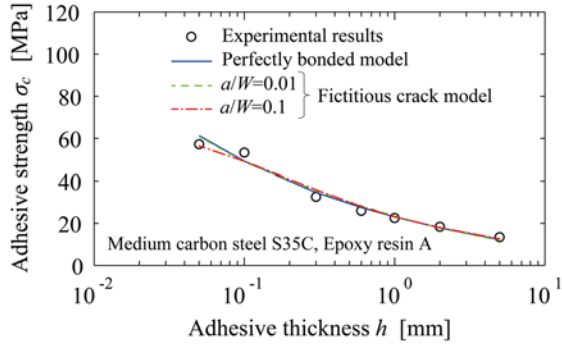
b
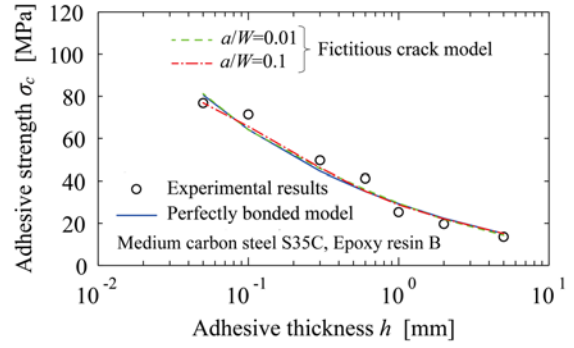
Fig. 23. Relationship between σ_c and h for bonded Medium carbon steel S35C. (a) Medium carbon steel S35C, Epoxy resin A, (b) Medium carbon steel S35C, Epoxy resin B.

a

b
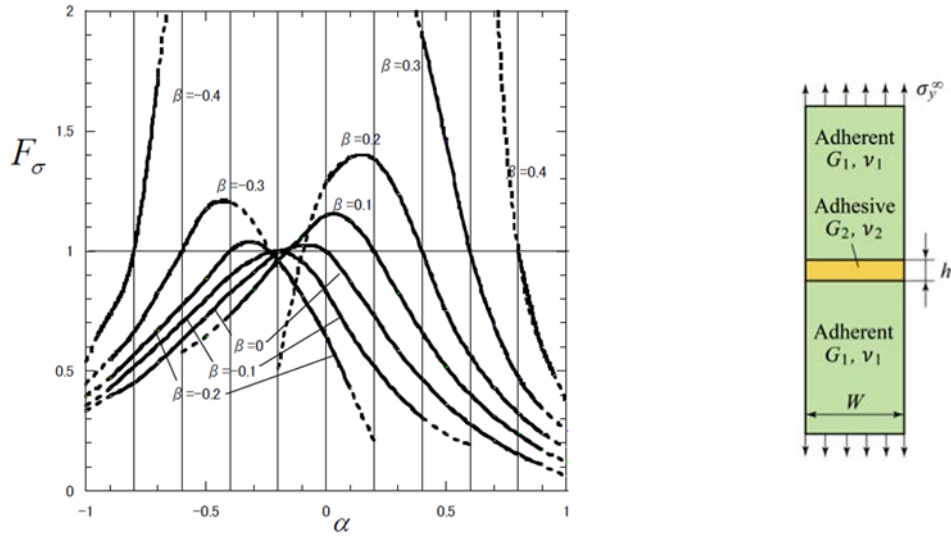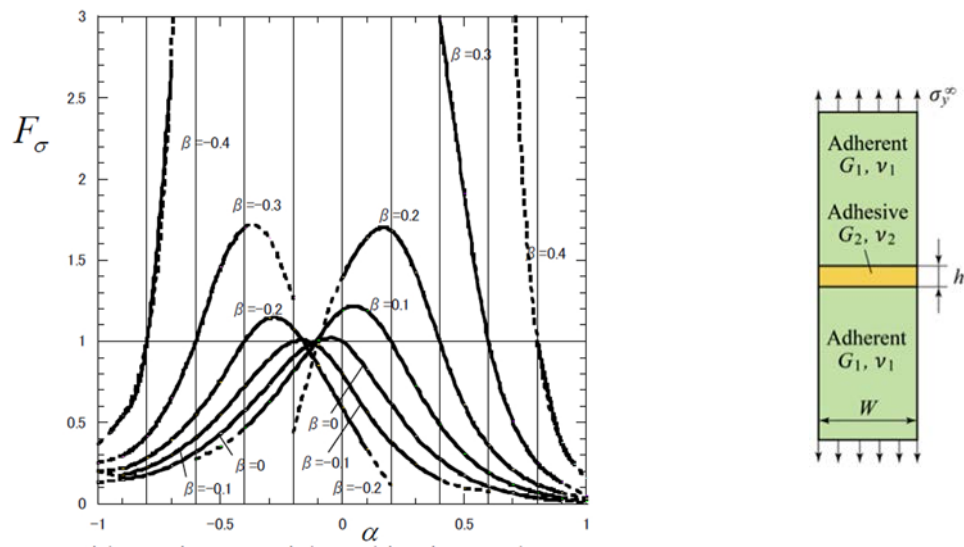
Fig.A.1. F_σ with varying material combination β when (a) $h/W = 0.001$; (b) $h/W = 0.1$.
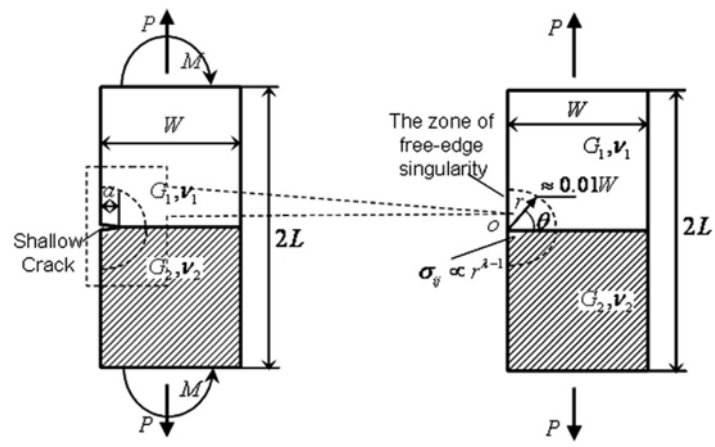
**Fig.B.1.** Shallow edge interface crack in a bonded strip.
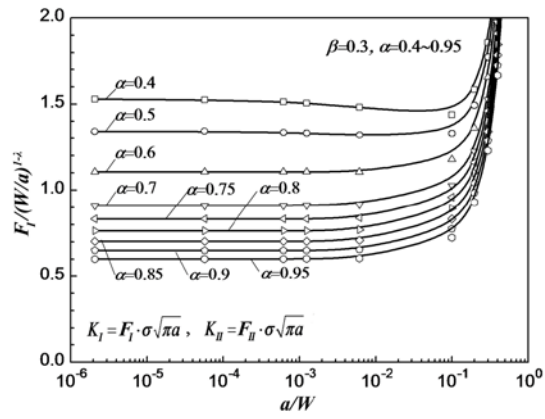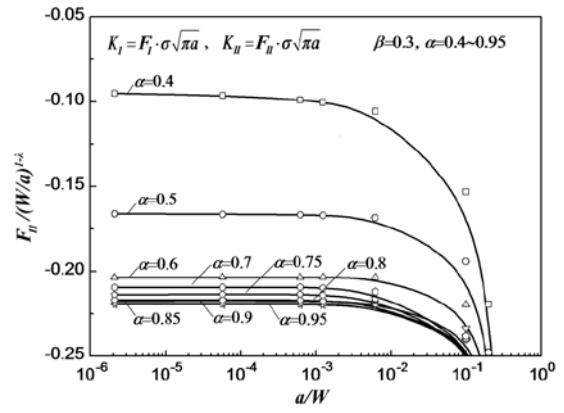
Fig.B.2. The values of $F_I / (W / a)^{1-\lambda}$ and $F_{II} / (W / a)^{1-\lambda}$ for $\beta = 0.3$.
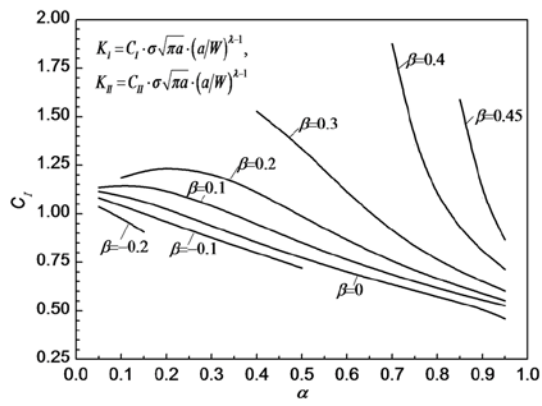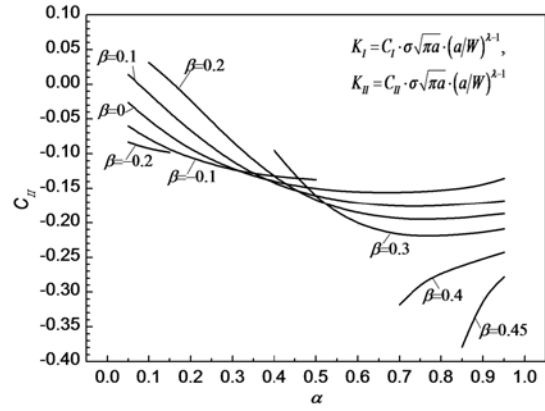
**Fig.B.3.** The values of C_I and C_{II} for various combination of materials.
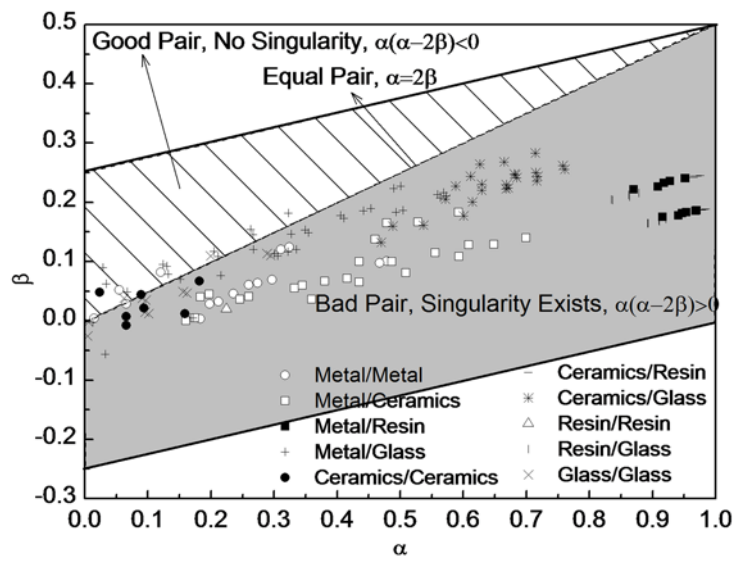
Fig.B.4. Dundurs' material composite parameters for several engineering materials.